Multi-timescale neural adaptation underlying long-term musculoskeletal reorganization.

(Multi-timescale neural adaptation)

*Roland Philipp[1,2], Yuki Hara[3], Naohito Ohta[1,2], Naoki Uchida[1,2], Tomomichi Oya[1,4], Tetsuro Funato[2], and *Kazuhiko Seki[1]

[1]National Center of Neurology and Psychiatry, Department of Neurophysiology, 4-1-1 Ogawa-Higashi, Kodaira, Tokyo 1878502, Japan
[2]University of ElectroCommunications, Graduate School of Informatics and Engineering, Dept. of Mechanical and Intelligent Systems Engineering. W2-217, 1-5-1 Chofugaoka, Chofu, Tokyo, Japan
[3]National Center of Neurology and Psychiatry, Department of Orthopaedic Surgery, 4-1-1 Ogawa-Higashi, Kodaira, Tokyo 1878502, Japan
[4]Western Institute for Neuroscience, University of Western Ontario, London, N6A 3K7, Canada

*Corresponding authors:
Kazuhiko Seki and Roland Philipp
Email: seki@ncnp.go.jp and roland@ncnp.go.jp

Author Contributions: R.P. and K.S. designed all experiments and wrote the paper. R.P., Y.H., N.U., and N.O. performed the experiments and analyzed the data. R.P., Y.H., T.O., and K.S. performed the surgeries. T.F. provided conceptual advice and wrote the paper. All authors reviewed the results and approved the final version of the manuscript.

Conflict of Interest Statement: The authors declare no competing interests.

Number of pages: 83 (92, including supplementary information)
Number of figures: 13 (18, including supplementary figures)
Number of multimedia: 7
Number of words for abstract: 173
Number of words in introduction: 706
Number of words in discussion: 1851

ABSTRACT

The central nervous system (CNS) can effectively control body movements despite environmental changes. While much is known about adaptation to external environmental changes, less is known about responses to internal bodily changes. This study investigates how the CNS adapts to long-term alterations in the musculoskeletal system using a tendon transfer model in non-human primates. We surgically relocated finger flexor and extensor muscles to examine how the CNS adapts its strategy for finger movement control by measuring muscle activities during grasping tasks. Two months post-surgery, the monkeys demonstrated significant recovery of grasping function despite the initial disruption. Our findings suggest a two-phase CNS adaptation process: an initial phase enabling function with the transferred muscles, followed by a later phase abolishing this enabled function and restoring a control strategy that, while potentially less conflicted than the maladaptive state, resembled the original pattern, possibly representing a 'good enough' solution. These results highlight a multi-phase CNS adaptation process with distinct time constants in response to sudden bodily changes, offering potential insights into understanding and treating movement disorders.

SIGNIFICANCE STATEMENT

After major changes to the body's mechanics, the nervous system adapts using strategies on multiple timescales. Our primate tendon transfer study shows that core muscle synergy groupings remain stable, reflecting a default to modular control. However, the activation of these synergies changes dramatically; an initial, rapid 'swap' of their timing proves to be **maladaptive**, impairing motor function. This conflict is only resolved through the gradual development of **slower, compensatory strategies** over several weeks. This process highlights the fundamental tension the CNS faces when its reliance on stable motor modules conflicts with the need for flexible control, offering insights into neural plasticity and staged rehabilitation.

Introduction

The central nervous system (CNS) continuously adapts bodily functions in response to both external and internal challenges. Experimental models based on external perturbations—such as altered gravitational fields or distorted sensory feedback—have illuminated mechanisms of sensorimotor adaptation (Sugita, 1996; Davidson and Wolpert, 2003; Luauté et al., 2009; Fleury et al., 2019). Because the changes in the external environment can be controlled by the experimental design, these models provide an opportunity to assess how the CNS adapts to them. However, the transient and predictable nature of these changes may not fully capture the demands posed by internal, long-lasting, and unpredictable alterations to the body's internal environment

In contrast, the internal changes such as developmental growth (Power and Schlaggar, 2017), fatigue (Green, 1997), postural sway (Zemková, 2022), and sensory disorientation (Schärli et al., 2024) impose distinct challenges. Because identifying the source, extent, and time-constant of changes in the internal environment is usually difficult, assessing the corresponding CNS adaptation is also challenging. Particularly, structural alterations to the musculoskeletal system—whether due to injury, disease, or surgery—fundamentally change the

body's biomechanics and sensorimotor associations, but the quantification of these changes is usually difficult. Accordingly, the way CNS remaps its motor control strategies corresponding to the changes is not yet well understood (Walker et al., 2004), although understanding such adaptations is crucial for elucidating the pathophysiology of motor impairments observed in chronic musculoskeletal conditions such as (Hunter and Eckstein, 2009) and muscular dystrophy (Mercuri and Muntoni, 2013).

To address this question, in this study, we employed a tendon transfer (TT) surgery model (Sperry, 1940), which introduces a controlled, sustained change to the musculoskeletal structure. TT surgery is a clinically well-established procedure (Gardenier et al., 2020) that surgically re-attaches the tendon of a specific muscle to that of a surrounding one. This procedure relocates a specific muscle, so that its contraction generates a new mechanical action and, consequently, novel somatosensory feedback. Because the internal change is controlled by the experimenter, the TT model provides a powerful platform to investigate how the CNS adapts to a new internal state. Another unique feature of TT model is that it places permanent changes of the internal environment while leaving the CNS anatomically intact. Unlike CNS lesion models (Hoffmann et al.,

2009) —where the injury itself disrupts neural circuits and thereby complicates the assessment of adaptive capacity of the CNS—TT offers a distinct advantage: it allows investigation of CNS-driven adaptation without the confounding effects of direct neural damage. Tendon transfer has been used in various species, with studies suggesting different adaptive capacities, ranging from limited adaptation in adult rodents (Sperry, 1940; Sperry, 1942; Slawinska and Kasicki, 2002; Bowlus et al., 2003) to more substantial adjustments in cats (Yumiya et al., 1979; Loeb, 1999) and primates, including humans (Lee and Seung, 1999; Wester et al., 2018; Gaetz et al., 2023). Therefore, adaptability to TT appears enhanced in primates and humans. Altogether, this approach provides a controlled platform to examine how the CNS adapts to musculoskeletal changes in primates.

According to earlier reports, there are two motor control strategies that could be involved when the CNS needs to face the sensorimotor remapping posed by structural alterations to the musculoskeletal system. First, the CNS may employ modular building blocks such as muscle synergies—coordinated activations of muscle groups that reduce the dimensionality of motor control (d'Avella et al., 2003; Bizzi and Cheung, 2013). Second, skilled behaviors like fine finger movements often require fractionation—the capacity to activate muscles

121 independently. When confronted with structural changes to the musculoskeletal
122 system, does the CNS adapt by modulating existing synergies, or by shifting
123 toward more fractionated control strategies?
124 This study aimed to identify long-term adaptive mechanisms of the primate CNS
125 following structural changes to the musculoskeletal system. We investigated
126 whether the CNS adapts by modulating existing muscle synergies or by altering
127 the fractionated control of muscles specifically affected by the surgical alteration.
128 We surgically altered the limb structure by performing crossed tendon transfers
129 of finger extensor and flexor muscle tendons. Using a trained finger-grasping task
130 as our behavioral readout, we examined how the CNS recalibrates muscle activity
131 to regain skilled motor function. Our findings provide new insights into the
132 dynamic reorganization of motor control following structural changes of the bodily.
133
134

RESULTS

In this study, we developed a novel crossed tendon transfer animal model. This involved surgically swapping the tendons of two antagonistic finger muscles in a macaque monkeys' forearm (Fig. 1). The effectiveness and consistency of the surgery was confirmed by measuring: (i) the distance traveled by muscle fibers and their intramuscular tendons in the transferred muscle (Fig. 2B, C); and (ii) the amount of fingertip displacement (Fig. 2D, E). Both measurements were induced by percutaneous electrical stimulation over the transferred muscles (Fig. 2A). For a detailed description of the results of these measurements see the Methods section. The two monkeys were assigned slightly different tasks, allowing us to examine controlled grasping in Monkey A and a more natural grasp in Monkey B (refer to the Methods section, and Figs. 3 and Fig. 4 for further details). The two monkeys ultimately performed related but distinct grasping tasks, a methodological divergence that provided a valuable opportunity to test the generality of the core adaptive mechanisms. Monkey A performed a controlled grasping task requiring a fine precision grip, designed to study adaptation of fine motor control (Fig. 3). While the same task was initially planned for both animals,

Monkey B performed this task inconsistently, frequently varying its grip strategy, and we could not reinforce this monkey to perform in single strategy consistently. Therefore, to ensure reliable task engagement and in accordance with the ethical principle of Reduction and Refinement (the '3Rs'; (Tannenbaum and Bennett, 2015)), the task for Monkey B was modified to a more naturalistic food retrieval grasp that the animal performed consistently (Fig. 4).

Once the monkeys had mastered their respective tasks, we recorded control sessions and then performed the crossed TT. Post-surgery, and once the monkeys had fully recovered and were able to perform the task independently (~3–4 weeks), EMG recordings and behavior were resumed.

Functional Recovery Follows a Period of Maladaptive Behavior

Despite the now reversed roles of the transferred muscles, the monkeys were able to recover their grasping performance within two months, assessed by both the return of key behavioral metrics to pre-surgical levels (Fig. 5A) and their consistent ability to perform the task independently (Supplementary Videos S3, S4, S7). However, this recovery was not immediate. The initial post-surgical period was instead defined by a phase of significant *maladaptation*, primarily

170 characterized by aberrant reaching. These aberrant movements included
171 inefficient, 'explorative' trajectories in Monkey A and target overshoots in Monkey
172 B (Supplementary Videos S2, S3, S6). This impairment was quantified across
173 two key behavioral metrics: grip formation times (Fig. 5A) and aberrant reaching
174 times (Fig. 5B). First, task-related grip formation times were significantly longer
175 immediately post-TT (Monkey A: 197.7 ± 92.2 vs. 660.6 ± 221 ms, $p = 0.014$;
176 Monkey B: 169.7 ± 14 vs. 316.3 ± 31.9 ms, $p = 0.016$); it took approximately 10
177 days for this metric to return to pre-TT levels and 20 to 32 days, respectively, to
178 stabilize. Second, the duration of the aberrant reaching component itself was
179 substantially elevated post-surgery. Monkey A exhibited these movements from
180 day 29 (1978 ± 715 ms) to 73 (93.4 ± 3.7 ms), while Monkey B showed them from
181 day 20 (103.4 ms) to 62 (107.6 ms), with the duration peaking at days 38-46 (167
182 ± 1.4 ms). Ultimately, overcoming these maladaptive behaviors restored
183 movement efficiency and precision, leading to the stabilization of grasping
184 performance by the end of the experimental period.
185
186

187 **A two-phase adaptation is observed in the EMG activity of individual**
188 **muscles**

189 Initially, we investigated whether EMG activity exhibited any changes post-TT.
190 Given that we interchanged the tendons of an antagonistic muscle pair,
191 functionally rendering the FDS an extensor and the EDC a flexor (as confirmed
192 mechanically, Fig. 2), a biomechanically sound adaptation would be to use the
193 former finger extensor (EDC) for finger flexion, and the former finger flexor (FDS)
194 for finger extension during a grasping task. We therefore analyzed EMG activity
195 from both transferred and non-transferred muscles to determine if these expected
196 functional changes occurred. Figure 6 shows a comparison of EMG activity
197 profiles for the two transferred muscles, EDC and FDS, in Monkey A (Fig. 6A–D).
198 Prior to surgery, the control showed distinct and contrasting EMG profiles in both
199 muscles. For instance, peak activity in EDC (▼) occurred long after completion
200 of the grasping action (indicated by vertical dashed lines at 0% task range) at
201 15% task time (Fig. 6A), coinciding with the animal pre-shaping its hand to
202 prepare for the subsequent grasp. Whereas peak activity in FDS (▽) was
203 observed immediately after completion of the grasping action (0.49%; Fig. 6C).
204 The question we posed was whether the post-surgery activity of EDC resembled

205 its original profile (without adaptation to surgery) or the activity of FDS (the
206 anticipated profile following surgical adaptation), and vice versa. Our findings
207 suggested that EMG activity patterns largely shifted in a manner consistent with
208 the new mechanical function imposed by the transfer. Early after TT, peak activity
209 of EDC occurred at -0.58% task time (Fig. 6B; days 29 [red line] and 64 [orange]),
210 which aligns with peak activity of FDS prior to TT (Fig. 6C; black line). Also, for
211 FDS, peak activity occurred at 11% task time (Fig. 6D; ▼), which aligned with
212 peak activity of EDC (Fig. 6A).
213 This was corroborated by the results in Monkey B (Fig. 6, panels K-M). Although
214 the EMG patterns of both muscles varied significantly as the two monkeys
215 performed different types of grasping actions, we found that the EMG of EDC
216 peaked at -6.12% before (Fig. 6K; ▼) and 0.35% and 1.05% after TT (Fig. 6L; ▽,
217 days 22 and 36, respectively), closely matching the timing for FDS control data
218 (Fig. 6M). The corresponding analysis for FDS could not be performed in Monkey
219 B, since the EMG signal of FDS was lost early after TT (see Methods for details).
220 We were able to extend our recordings to 122- and 64-days post-TT for monkeys
221 A and B, respectively. This allowed us to examine whether the adaptations
222 observed in the early period were consistent throughout the experimental period.

223 These additional days (Fig. 6B, D; 69 [cyan], 79 [blue], and 99 [black] post-TT;
224 see Fig. S1 for recordings from all days) showed that the EMG activity profiles for
225 both muscles unexpectedly returned to their pre-surgery state. For example, as
226 already described, the EMG signal of EDC at days 29 and 64 shared the
227 characteristics of FDS, but by the following day (only 5 days later, day 69 [light
228 blue] post-TT) already exhibited pre-TT characteristics of EDC, continuing as
229 such until the end of the recording period (day 79 [blue] and 99 [black]). This was
230 confirmed for the EDC muscle of Monkey B (Fig. 6K, L; Fig. S1U-AO for
231 recordings from all days).
232 Figure 6G illustrates cross-correlation coefficients between the EDC EMG profile
233 post-TT (EDC-post) and the original EDC control data (EDC-pre) in Monkey A.
234 Figure 6I shows coefficients for EDC-post and FDS-pre correlations in the same
235 monkey. The coefficient corresponding to the original profile decreased to
236 between -0.3 and 0.2 over approximately 65 days (Fig. 6G). In contrast, the
237 coefficient corresponding to the expected EMG profile exhibited an inverse
238 pattern, with low coefficients pre-TT and a high coefficient (of 0.9) post-TT (Fig.
239 6I). Cross-correlation analysis for FDS (Fig. 6H, J) revealed a similar pattern.
240 Cross-correlation coefficients for FDS-pre- vs. FDS-post-analysis declined from

241 1 to negative values, only to rebound to their original values within a month (day
242 79; Fig. 6H). This outcome aligns with our previous observations (Fig. 6B, D), and
243 were corroborated by the results from Monkey B (Fig. 6K-Q). Here, cross-
244 correlation coefficients dropped from +0.95 to +0.1 for EDC-pre vs. EDC-post
245 comparison, and increased from -0.5 to 0.9 for the FDS-pre- vs. EDC-post
246 comparison (Fig. 6P, Q). After 42 days post-TT, cross-correlation coefficients
247 started to gradually increase or decrease to +0.9 and -0.7, respectively. This
248 indicates that the anticipated initial changes in EMG activity profiles are not
249 permanent. Instead, they revert to their original patterns two months post-TT.
250 Interestingly, changes in EMG pattern were not isolated to the transferred
251 muscles; non-transferred muscles exhibited a variety of complex adaptations
252 (Figs. 6, S1-S3). Many agonists adapted in concert with their transferred synergist,
253 following the same two-phase "swap-and-revert" pattern seen in Figure 6. In
254 Monkey A, these included extensors ED23 and ECU, while in Monkey B, they
255 included ED23, ED45, and ECU (see Fig. S1 for details). In contrast, other
256 muscles showed patterns that were incompatible with a simple swap. For
257 example, the non-transferred flexor carpi radialis (FCR) in Monkey A showed a
258 distinct adaptive profile characterized by a drastic initial decrease in one activity

259 peak and a consistent increase in a later peak (Fig. 6E, F). A similar incompatible
260 pattern was seen in palmaris longus (PL) (Fig. S1H, I, R, S). Finally, some
261 muscles, like the extensor carpi radialis (ECR) in Monkey B, remained relatively
262 stable post-surgery (Fig. 6N, O).
263

264 **Adaptation occurs through modulating the activation of stable muscle**
265 **synergies**

266 Alternation of EMG activity in non-transferred muscle suggests one possibility:
267 TT might alter the control strategy of coordinated muscle activity for hand
268 movement by modifying the transferred muscles and their agonists as a cohesive
269 unit (i.e., muscle synergy). To test this, we conducted a similar analysis on
270 temporal activation coefficients of muscle synergies. We computed synergy
271 weights (Fig. 7A, B and Fig. 8C, G for Monkey A; and Fig. 7E, F and 8 D, H for
272 Monkey B) and temporal activation coefficients (Fig. 7 C, D and Fig. 8 E, I for
273 Monkey A; and Fig. 7 G, H and Fig. 8 F, J for Monkey B) from EMGs using non-
274 negative matrix factorization (NMF) (Lee and Seung, 1999). We extracted four
275 muscle synergies that accounted for more than 80% (Cheung et al., 2012) of the
276 'variance accounted for' (VAF) (Figs. 8A, B, 85% for both monkeys; the results of

the original and shuffled data sets are shown). Among these synergies, one was a finger flexor synergy and another was a finger extensor synergy, identified before the crossed tendon transfer in each monkey (Fig. 7A, B, E, F and Fig. S4). These were referred to as synergy A and synergy B, respectively.

We examined if the composition and activation coefficient of each synergy changed, corresponding to the changes observed in the transferred and non-transferred muscles. First, we analyzed changes in the composition of these synergies. The cosine distance for the same synergy pairs (e.g., synergy A of pre-TT and synergy A of post-TT in all recording days (Fig. S4A, E; monkey A and B, respectively) was low (mean [± SD]: 0.03 [± 0.03] in Monkey A and 0.09 [± 0.11] in Monkey B) and different pairs (e.g., synergy A of pre-TT and synergy B of post-TT) was high (mean [± SD]: 0.67 [± 0.08] in Monkey A and 0.61 [± 0.14] in Monkey B). There was a one-to-one correspondence between synergy pairs ($p < 0.0001$, two-way analysis of variance [ANOVA] due to synergy factor; $p < 0.01$, Bonferroni post-hoc test between synergy of the same pair and different pair). This was demonstrated in both monkeys (S4A-D and E-H for monkey A and B, respectively). These results indicate that the composition of these four

294 synergies and the contribution of each muscle do not change drastically before
295 and after TT surgery.
296 Second, we analyzed changes in the activation coefficients of these synergies.
297 Prior to TT, the activation coefficients for the flexor synergy (synergy A) reached
298 a peak at +0.97% (Fig. 7C). Post-TT, these coefficients shifted towards later times
299 shortly after surgery (+10.7%), but eventually returned to their original timing.
300 Meanwhile, the extensor synergy (synergy B) peaked at 12.62% pre-TT and
301 moved to -0.97% shortly after surgery. Like the flexor synergy, the extensor
302 synergy also reverted to its original timing in subsequent sessions (Fig. 7D).
303 These characteristics corresponded well to the ones found in the transferred
304 muscles (Fig. 6), supporting our hypothesis that the transferred muscle and its
305 agonist changes as a cohesive unit.
306 Figure 8E shows the temporal changes for synergy C, a wrist flexor synergy (Fig.
307 8C and S4C). While two peaks were observed prior to surgery (+1.46% and
308 +15%), the early post-surgery sessions did not exhibit any significant peaks.
309 However, later sessions displayed a single peak at +14.6% task time, with an
310 increasing magnitude as a function of recovery days. These characteristic
311 changes corresponded well to a patten that was incompatible to the transferred

312 muscles found in FCR and PL, as described above. Indeed, both muscles
313 showed highest synergy weights for this synergy (Fig. 7C and S4C). Synergy D
314 was a wrist extensor synergy (Fig. 8G and S4D), and underwent a single notable
315 change on day 29, but quickly reverted to its original pattern (Fig. 8I). These
316 pattens of changes in synergy 3 and 4, both contributed minimally to the EMG of
317 transferred muscles. This suggests that some non-transferred muscles change
318 their EMG activity following the mode, which is independent to the one observed
319 in the transferred muscle and may reinforce the functional adaptation made by
320 the transferred muscle and its synergists.
321 Several of these results were also confirmed in Monkey B. Activation coefficients
322 of extensor synergy B peaked at -8.75% before TT, increasing to +3.5% after TT
323 (Fig. 7G). This peak activity persisted until the last day (day 69 post-TT), when it
324 shifted back to an earlier time than -10% of the task range. This pattern
325 corresponds well to that found in the transferred muscles (EDC; Fig. 6K, L).
326 Again, the characteristics of these changes in activation coefficients of muscle
327 synergies were also quantitatively confirmed by cross-correlation analysis of all
328 four muscle synergies in both monkeys. The coefficients were plotted over the
329 course of experimental days in relation to tendon surgery (Fig. 9). In this analysis,

330 the activation coefficient of each synergy was cross-correlated with either the one
331 from synergy A (finger flexor synergy; Fig. 9C, D, G, H) or synergy B (extensor
332 synergy; Fig. 9A, B, E, F) before TT. As previously demonstrated for the FDS and
333 EDC muscles, the temporal activation coefficients of muscle synergies A and B
334 (flexor and extensor) displayed a distinct pattern. After cross-correlation with their
335 own control data, both the flexor and extensor synergies showed coefficients of
336 1 prior to surgery. These became negative for 66 days post-surgery before
337 reverting close to their original values (Fig. 9B, C). However, after cross-
338 correlation with control data of the antagonistic muscle synergy (i.e., extensor for
339 flexor synergy and vice versa, Fig. 9B, D), the pattern was reversed. Coefficients
340 started with negative values prior to TT and shifted to positive coefficients near 1
341 shortly after surgery. Around 66 days later, the correlation coefficients returned
342 to negative values. In short, these results mirror our findings between the
343 transferred muscles (Fig. 6G, H). For synergies C and D, the changes in cross-
344 correlation coefficients over time were markedly different. For synergy C,
345 coefficients begin to steadily increase when cross-correlated with control data of
346 the extensor synergy (synergy B, Fig. 10E), and decreased with the flexor
347 synergy (synergy A, Fig. 10G). This suggests an increasing contribution to finger

extension. In contrast, synergy D does not exhibit any specific pattern following TT.

In Monkey B, this cross-correlation analysis revealed a more varied, or differential, pattern of adaptation across the four synergies (Figs. 9 and 10). The primary extensor, Synergy B, mirrored the results in Monkey A, showing a clear swap-and-revert pattern (Fig. 9F, H). In contrast, Synergy A did not show a clear reversal; its correlation coefficients gradually converged towards zero, likely due to the absence of the FDS EMG signal in the analysis (Fig. 9E, G). Of the secondary synergies, Synergy C showed no discernible trend (Fig. 10E, G), while Synergy D exhibited a complex pattern of an immediate change, a quick reversion, and a second gradual change late in the adaptation period (Fig. 10F, H).

In summary, both monkeys exhibited a distinct two-phase adaptation following TT. We define the 'early phase' as the period from initial post-surgical recovery up to the reversal of the swapped activation patterns (approximately days 20/29 to ~65 post-TT, see Fig. 9), characterized by the transferred muscles/synergies adopting antagonistic temporal profiles. The 'late phase' encompasses the period following this switch-back (after ~day 66 post-TT), where original activation timings were largely restored.

366 **The Early Adaptation Phase is Characterized by a Maladaptive Neural and**

367 **Behavioral Profile**

368 The early adaptation phase was defined by a distinct neural strategy that

369 correlated with significant behavioral deficits. First**,** the period dominated by

370 aberrant reaching movements and prolonged grip times (Fig. 5B) was precisely

371 when the swapped activation of Synergy A and B was most prominent (Fig. 9).

372 This temporal link provides strong evidence that this initial 'swap' strategy was, in

373 fact, maladaptive, as the flawed neural control directly underpinned the

374 impairments in movement efficiency and precision.

375 Second, we found that the net activity of muscles representing certain muscle

376 synergies (aggregated average EMG; aaEMG) showed distinct, synergy-specific

377 changes over time (Fig. 11). A key difference was observed in the finger extensor

378 synergy (Synergy B). In Monkey A, this synergy demonstrated what we term a

379 neuromuscular 'arms race': a steady and significant increase in aaEMG post-TT

380 until day 64 ($p < 0.0001$) as the CNS appeared to escalate activation to overcome

381 the internal conflict between the transferred EDC (now a flexor) and its non-

382 transferred synergists (which remained extensors), before abruptly reverting to

383 its pre-TT level (Fig. 11B, F). In contrast, while Monkey B also showed a

384 significant initial surge in Synergy B activity (day 22: $p < 0.0001$), this was
385 followed by a gradual return to baseline and below (day 64: $p < 0.001$), lacking a
386 sustained 'arms race' (Fig. 11J, N). This discrepancy is likely attributable to the
387 different force requirements of the tasks. The 'arms race' in Monkey A may have
388 been driven by the need to generate high grip force against the synergy's internal
389 conflict, whereas Monkey B's delicate food-retrieval task did not require such high
390 forces, thus lacking the same drive for escalating, energetically costly activation.
391 For the finger flexor synergy (Synergy A), Monkey A showed a general decrease
392 in activity ($p = 0.0004$ at day 79; Fig. 11A, E), while Monkey B showed a
393 consistent and significant increase throughout the experiment (day 22: $p =$
394 0.0004; day 64: $p = 0.0008$). This was expected, as Monkey B's Synergy A relied
395 on FDP and PL to compensate for the loss of FDS function (Fig. 11I, M). Synergy
396 C exhibited a general increase in activity during the post-TT phase in both
397 monkeys (Fig. 11G, O), while Synergy D showed no significant differences in
398 Monkey B and only minor changes in Monkey A (Fig. 11H, P). All statistical
399 comparisons were made against the pre-surgery control period using a two-
400 sample t-test with Bonferroni correction ($\alpha = 0.01$).

Taken together, these distinct patterns of aggregated EMG activity—especially the escalating, conflicted activation in Synergy B—further illustrate that the early adaptive phase was characterized by an unstable and inefficient neural control strategy.

Recruitment of a Compensatory Tenodesis Strategy Enables Late Adaptation

The development of a compensatory strategy, primarily involving the wrist flexor synergy (Synergy C), appears crucial for enabling the final phase of adaptation. The increasing contribution of this synergy is supported by cross-correlation analysis, which shows that the correlation between Synergy C and the extensor synergy (Synergy B) steadily increased over time after an initial drop (Fig. 10A; $p < 0.05$, two-sample t-test). Increased reliance on synergy C following TT suggests a compensatory strategy to overcome the difficulty in finger extension, crucial for grasping. This is despite the recruitment of the finger extensor and wrist flexor synergies, which seemed inadequate to achieve effective flexion. The interactions between the cumulative proximal-to-distal joint angles and musculo-tendon length can be complex. In our experiments, as in human patients who

419 receive tendon transfers (Zajac, 1992), those interactions can affect the ranges
420 of finger flexion-extension that can be achieved for a given wrist angle (i.e.,
421 passive and active tenodesis). Briefly, biomechanically, wrist flexion can enable
422 finger extension (i.e., a dynamic tenodesis where extensor tendons of the fingers
423 cross both the wrist and interphalangeal joints): Finger extension can cancel out
424 the increase in total musculo-tendon length produced by wrist flexion. This
425 compensatory interaction across joints allows for some degree of functional hand
426 use, even in the absence of active finger movement (Cash and Jones, 2011) (see
427 the Discussion for a complete description).
428 Further kinematic analysis of Monkey B (Fig. 12; no analysis on Monkey A due
429 to low-resolution video images) indicated that this monkey indeed exhibited a
430 similar active tenodesis as human patients. The angle at the
431 metacarpophalangeal (MCP) joint, responsible for finger extension, steadily
432 increased (Fig. 12A) after surgery, indicating finger extension. Concurrently, the
433 wrist joint angle decreased (Fig. 12B), indicating wrist flexion. This coordinated
434 movement suggests a compensatory strategy to achieve finger extension during
435 grasping. Statistical analysis confirmed that MCP and wrist joint angles differed
436 significantly between pre- and post-TT ($p < 0.0001$, ANOVA; $\alpha = 0.01$). Therefore,

we suggest that deteriorated finger extension after TT was assisted by a compensatory wrist flexion synergy.

Discussion

The central nervous system's (CNS) response to profound musculoskeletal change is a fundamental problem in motor control. This study sought to determine whether the primate CNS adapts to such change by flexibly modulating stable muscle synergies or by developing more fractionated, independent muscle control. We found that the CNS initially defaulted to a modular strategy, repurposing entire synergies by swapping their activation timings. This simple solution, however, proved to be maladaptive, creating a mechanical conflict that impaired motor function. This early maladaptive phase was ultimately resolved through the gradual development of compensatory movements, leading to a "good enough" functional recovery. This multi-stage process, operating on different timescales, highlights the intricate balance between modularity and flexibility in neural adaptation.

The CNS Defaults to a Modular Strategy, Leading to a Maladaptive Conflict

Our primary finding provides a direct answer to the question posed in the introduction: the CNS adapted to the tendon transfer not by developing fine-grained, fractionated control, but by implementing a modular strategy by

461 repurposing entire co-activation modules (Overduin et al., 2008; Berger et al.,
462 2013; Bizzi and Cheung, 2013; Takei et al., 2017). The initial and most immediate
463 neural change was a wholesale swap of the temporal activation patterns of the
464 primary flexor and extensor synergies (Synergy A and B). The fact that the
465 muscle weight compositions of all four synergies remained remarkably stable
466 throughout the months-long experiment (Fig. S4), in the face of drastically altered
467 biomechanics, strongly supports the hypothesis that these synergies represent
468 stable, neurally constrained building blocks (d'Avella et al., 2003; Bizzi and
469 Cheung, 2013; Takei et al., 2017). Our result indicated that this modular approach
470 is likely the default for adaptation to altered musculoskeletal systems because it
471 is computationally "easy" and metabolically "cheap" (Flash and Sejnowski, 2001).
472 It relies on the simple retiming of pre-existing, stable neural circuits—thought to
473 be encoded in the spinal cord and brainstem—which is a far less demanding
474 operation than the "difficult" alternative of fractionated control (Bizzi and Cheung,
475 2013). The latter would require extensive synaptic plasticity and cortical
476 remapping to selectively uncouple muscles that were previously co-activated, a
477 process associated with the slower, more deliberate learning of an entirely new
478 motor skill (Kitago and Krakauer, 2013). Thus, the simple and economical

479 strategy is prioritized in the CNS to deal with an acute alteration of the musculo-
480 skeletal system.

481 However, this adherence to established synergy structures created a
482 fundamental conflict. Activating the original extensor synergy (Synergy B) after
483 the transfer now inevitably co-activated the surgically transferred EDC, which
484 functioned mechanically as a flexor, alongside non-transferred muscles like ED23
485 and ECU, which remained anatomical extensors. This internal mechanical
486 antagonism appears to be the root cause of the early maladaptive phase. This
487 interpretation is supported by two key lines of evidence from our results. First, the
488 period of severe behavioral impairment, characterized by aberrant reaching and
489 inefficient grasping (Fig. 5B), occurred precisely when this flawed "swap" strategy
490 was active. Second, the aggregated EMG activity revealed a sustained and
491 significant increase in the total activation of the conflicted Synergy B in Monkey
492 A (Fig. 11B, F), likely reflecting an energetically costly effort to overcome the
493 internal mechanical antagonism. This scenario can be viewed through the lens of
494 optimal control and cost-benefit analysis, where a cost function is minimized
495 (Wolpert, 1997). The initial "swap" strategy, while computationally cheap to select,
496 incurred an unacceptably high operational cost in terms of both poor task

performance (high error) and excessive energy expenditure. It was this profoundly unfavorable cost-benefit ratio that likely served as the critical error signal that drove the CNS to abandon this initial strategy.

Resolution Through Slower Compensatory Adaptations

The CNS did not persist in the failed swap-based strategy. The high metabolic and computational cost of activating a mechanically conflicted synergy likely triggered the second rapid adaptation: the "switch-back" of synergy activation timings toward their original patterns (Fig. 7, 9). This rapid reversion, occurring over just a few days, is characteristic of an error-based learning mechanism, a form of adaptation that is profoundly impaired by cerebellar damage across a range of tasks, including adaptation to force fields (Smith and Shadmehr, 2005), prismatic shifts (Martin et al., 1996), and split-belt treadmills (Morton and Bastian, 2006). It is plausible that the CNS operates with an implicit threshold for an acceptable cost/performance ratio; once the persistent task failure and high muscular co-contraction of the swap strategy exceeded this threshold, a swift recalibration was initiated. This reversion, despite the remaining mechanical antagonism from the transferred tendons, represents a "good enough" solution

514 where functional success is prioritized over perfect efficiency (Mussa-Ivaldi and
515 Bizzi, 1995; Ranganathan et al., 2013; Gijsberts et al., 2014). The rapid timescale
516 of this change is highly consistent with the cerebellum's proposed role as a
517 forward model, predicting the sensory consequences of motor commands and
518 driving rapid learning in response to sensory prediction errors (Popa et al., 2016).

519 Crucially, this switch-back to a less conflicted state, presumably representing the
520 involvement of the error-based learning process, was likely enabled only by the
521 concurrent development of slower, compensatory strategies that provided an
522 alternative means to achieve the task goal. The primary compensation was a
523 learned use of the tenodesis effect. Over weeks, the monkeys gradually
524 increased the activation of the wrist flexor synergy (Synergy C) during hand
525 opening. This wrist flexion biomechanically generates passive finger extension
526 (Zajac, 1992; Cash and Jones, 2011), providing a viable new method for hand
527 pre-shaping. This learned, compensatory behavior, confirmed by kinematic
528 analysis (Fig. 12), ultimately allowed the CNS to abandon the maladaptive
529 synergy swap. This gradual, exploratory process is distinct from the following
530 rapid adaptation and represents a form of motor skill acquisition, a process which

may be associated with plasticity in cortical structures like the motor cortex and basal ganglia. (Kitago and Krakauer, 2013).

This multi-timescale process, conceptually summarized in Figure 13, aligns well with influential two-state models of motor learning, which propose parallel "fast" and "slow" learning systems (Smith et al., 2006a). These models posit that a fast system responds strongly to error but has poor retention, while a slow system responds weakly to error but retains information well, enabling robust long-term memory. The initial synergy swap and subsequent "switch-back" appear to be governed by the fast system (likely cerebellar), which responds strongly to error but has poor retention. The gradual learning of the tenodesis effect is the signature of the slow system (likely cortical and/or basal ganglia-dependent), which integrates experience over a longer period to build robust, lasting skills (Trewartha et al., 2014). The interaction between these systems is key: as the slow system gradually develops the effective tenodesis compensation, it reduces the overall task error. This reduction in error removes the primary drive for the fast, error-correcting system to continue its search for a solution. With its error signal quieted, the fast system allows the control policy to stabilize, and the CNS "settles" into the "good enough" compensatory state. This suggests a control

549 architecture where the successful output of a slow, deliberate skill-learning
550 system can gate and ultimately supersede the output of a fast, reactive adaptation
551 system, leading to a stable and functional long-term motor plan.
552

553 **Broader Implications and Limitations**

554 Our findings reveal a complex interaction between adaptive processes operating
555 on different timescales. The initial, rapid synergy swap may be linked to a
556 'sensory surprise' from altered proprioceptive feedback (Kitazawa et al., 1995;
557 Martin et al., 1996; Smith et al., 2006b; Edwards et al., 2012; Petitet et al., 2018),
558 driving a fast but flawed response. This multi-level network reorganization
559 presents a more complex challenge than the gain modulation within single or
560 specific CNS pathways seen in studies of spinal reflex conditioning (Thompson
561 and Wolpaw, 2014). Further understanding the interaction between the global
562 synergy reorganization observed in this study and the underlying local
563 sensorimotor loops will require considering factors not assessed here, such as
564 the roles of spinal reflex pathways (Smith et al., 2006c) and fusimotor drive
565 (Vallbo et al., 1979; Hospod et al., 2007). The altered biomechanics would have
566 immediately changed proprioceptive feedback, triggering rapid modulation of

spinal reflex circuits and requiring recalibration of the fusimotor system, which adjusts muscle spindle sensitivity via alpha-gamma co-activation. A comprehensive model must ultimately connect the global synergy reorganization with these local, interacting feedback and control loops.

While our primary analysis focused on the grasping, the adaptation encompassed the entire reach-to-grasp sequence, as evidenced by the initial deficits in reaching movements (Supplementary Videos S2, S3, S6; Fig. 5B). The observation that both monkeys, engaged in both a highly controlled learned task and a more naturalistic grasping task, showed similar adaptive patterns strengthens the generalizability and ecological validity of our findings (Berniker et al., 2013). Furthermore, the qualitative reports of proficient real-world hand use indicate that the learned compensatory strategies were not narrow "tricks" but robust solutions that transferred to unconstrained activities, demonstrating their "portability" to the complexities of natural behavior.

However, a limitation is that this generalization was not tested systematically. Another critical point is that our paradigm cannot distinguish between the unlearning of a maladaptive strategy and the relearning of a functional one. This distinction is crucial for both motor memory theory and clinical practice (Kitago et

al., 2013). The disappearance of the initial "swap" strategy could be due to passive decay (forgetting), active inhibition of the memory (extinction), or the formation of a new, stronger memory that outcompetes it (interference) (Villalta et al., 2013). The literature increasingly suggests that unlearning is an active process, and that the new, successful compensatory strategy likely supplants the maladaptive one through interference. This question is vital for rehabilitation: should therapy focus on "erasing" bad habits, or on intensively training better ones to overwrite them? Our results lend weight to the latter, suggesting functional recovery is a process of competitive memory formation.

Implications for Sensorimotor Rehabilitation

These findings may hold implications for sensorimotor rehabilitation. The observation of a distinct maladaptive phase followed by compensation and recovery suggests a staged approach could be beneficial (Hatem et al., 2016; Kakavas et al., 2025). An early phase of therapy might focus on minimizing sensory prediction errors caused by the altered proprioceptive feedback, and reducing maladaptive responses through techniques aimed at integrating the altered body schema (e.g., using visual feedback or task-oriented practice) (Nudo

et al., 1996; Takeuchi and Izumi, 2012; Zeiler and Krakauer, 2013; Foell et al., 2014; Levin et al., 2015; De Nunzio et al., 2018; Sattin et al., 2023; van Vliet et al., 2023). This stage would guide the fast, error-driven learning system. A later phase could then employ task-specific training to promote effective compensatory strategies, facilitating the abandonment of maladaptive patterns and the consolidation of a stable motor strategy (Murata et al., 2008; Maier et al., 2019). This second stage engages the slow, skill-acquisition system by creating a rich, problem-solving environment. Finally, a third stage would focus on intensive, high-repetition practice to automate the new functional motor plan, making it robust for real-world use through dosage and generalization (Winterbottom and Nilsen, 2024). This neurobiologically-informed staging—guiding fast adaptation, then facilitating slow skill learning, then driving consolidation—may offer a more logical and effective path to functional recovery.

619 **METHODS**

620 ***Animals***

621 Data were collected using two male macaque monkeys (*Macaca fuscata*; Monkey
622 A: 7.8 kg and Monkey B: 9.9 kg) purpose-bred at the National Bioresource Project
623 (NBRP). They were kept in custom-made primate cages, allowing for potential
624 pair housing. Both monkeys were trained to perform a simple grasping task.
625 During experimental recordings, the monkeys were seated in a primate chair
626 without further restraint. Their head movement remained unrestricted at all times.

627

628 ***Procedures***

629 All procedures were designed to minimize discomfort and pain and approved by
630 the institutional Animal Care and Use Committees at the National Center of
631 Neurology and Psychiatry (NCNP), Tokyo, Japan. Details of the surgical
632 operations, experimental setup, and procedures for electromyography (EMG)
633 recordings have been previously described (Takei and Seki, 2010).

634
635

636 ***EMG implant surgery***

637 Both animals were familiarized with the experimental setup and trained to perform
638 the behavioral task prior to surgery. After an initial training period, EMG
639 electrodes were chronically implanted subcutaneously into several muscles of the
640 left forearm including the FDS, FDP, and EDC (Figs. 1, 3C, and 4C). Individual
641 muscles were localized and confirmed using electrical microstimulation before
642 implanting EMG electrodes chronically by two methods. For muscles involved in
643 the crossed tendon transfer procedure, muscle fascia was cut and EMG wires
644 with looped ends were placed on top of the muscle belly. These were then
645 secured by reclosing the fascia with absorbable suture threaded through the loop
646 (AS-361, stainless-steel Cooner wire, Conner Wire Co., Chatsworth, CA, USA).
647 All other muscles were directly implanted into the muscle belly using a 22-gauge
648 hypodermic needle. Each wire was threaded into the needle tip, folded back along
649 the shaft, and inserted into the muscle before carefully retracting the needle.
650 Electrode separation for bipolar recordings was approximately 5–10 mm. Note
651 that some EMG recording sites were lost over time. Surgical procedures were
652 carried out under deep general anesthesia (sevoflurane 1.5 to 2.5% in 2:1
653 O2/N2O) and with full aseptic precautions. Heart rate, blood pressure, body

654 temperature, and blood oxygen saturation were monitored throughout surgery.
655 Analgesics and antibiotics were administered intramuscularly for at least one
656 week postoperatively.
657

658 ***Tendon-Transfer Surgery***

659 After a minimum four-week recovery period from EMG implant surgery, TT
660 surgery was performed. The FDS and EDC tendons were cut as distally as
661 possible (immediately below and above the wrist for FDS and EDC, respectively)
662 to avoid damaging the Golgi tendon organ located near the junction between the
663 muscle fibers and tendon (Schoultz and Swett, 1972; Jami, 1992). Tendons were
664 then guided either through the gap between the radius and ulnar bone (Monkey
665 A), or around the wrist and then re-attached to the tendon of the antagonist
666 muscle using a tendon graft harvested from the plantaris tendon of the lower limb
667 (Monkey B; EDC → FDS: direct connection; and FDS → EDC: tendon grafting).
668 This was only necessary in Monkey B since the tendons used for the cross-
669 transfer were too short. This surgical procedure aimed to reverse the primary
670 mechanical actions of the manipulated muscles, making the FDS tendon an
671 effective finger extensor and the EDC tendon an effective finger flexor. The

672 success and nature of this mechanical rearrangement were verified post-
673 operatively via direct muscle stimulation (see Methods subsection 'Tendon
674 transfer confirmation' and Fig. 2). The general organization and function of the
675 major forearm muscles involved in finger flexion and extension in *Macaca fuscata*
676 are broadly comparable to those in humans (Vanhoof et al., 2021; Yan et al.,
677 2022).

678 Surgical procedures were carried out under deep general anesthesia
679 (sevoflurane 1.5 to 2.5% in 2:1 O_2/N_2O) and with full aseptic precautions. Heart
680 rate, blood pressure, body temperature, and blood oxygen saturation were
681 monitored throughout surgery. Analgesics and antibiotics were administered
682 intramuscularly for at least one week postoperatively. Both monkeys wore a
683 plaster cast post-surgery, but its effectiveness was limited (lasting approximately
684 one week).

685

686 ***Tendon transfer confirmation***

687 To verify the success and long-term stability of TT surgery, two procedures (Fig.
688 2) were implemented. During the first procedure, the monkey was sedated and

689 its arm was secured to a metal frame (Fig.2A). Electrical stimulation was then
690 applied to either the FDS or EDC muscle (50 mA, DS8R, Digitimer, Welwyn
691 Garden City, UK), while ultrasound scans of tendon movements were
692 concurrently captured (SONIMAGE MX1, Konica Minolta, Inc., Tokyo, Japan
693 (Nordez et al., 2009; Dieterich et al., 2017).

694 Figure 2B shows a sonogram of the FDS muscle and its intramuscular tendons.
695 The left side displays a static image of the FDS muscle at a specific moment, with
696 white arrows indicating the FDS tendon used for measurement. The right side
697 shows staggered images (top white box) of the FDS tendon displacement
698 triggered by muscle stimulation. The lower right inset illustrates the measurement
699 area. The displacement wave area represents the intensity of muscle contraction,
700 and was calculated by measuring the average duration (a, in seconds) and
701 amplitude (b, in cm) of three successive waves. The area (a*b/2) and regression
702 line for FDS (red) and EDC (blue) (R^2 > 0.5 for FDS) for days 0, 7, and 105 post-
703 TT are shown (Fig. 2C). The results suggest that the muscle contractions induced
704 by direct electrical stimulation remained nearly constant.

705 For the second procedure, high-speed videos (37U Series Color Industrial
706 Camera, The Imaging Source, Charlotte, NC, USA) of the monkey's finger
707 movements were recorded while electrically stimulating the FDS or EDC. Markers
708 were placed on the nails of the index, middle, and ring fingers (Fig. 2A) to
709 measure finger displacement in xyz-dimensions using DeepLabCut software
710 (Mathis et al., 2018; Nath et al., 2019). The sum of Euclidean distances of each
711 marker from the origin of the three-dimensional (3D) coordinate system was
712 computed as a scalar quantity. Post-surgery, movement along the z-axis
713 reversed, indicating a shift from finger flexion to extension due to TT (Fig. 2D;
714 blue: pre-TT on surgery day, dark brown: post-TT on surgery day, light brown: 1
715 wk post-TT, and red: 3 wk post-TT). The scalar quantities of each finger did not
716 significantly change during muscle stimulation on days 0-, 7-, and 105-days post-
717 TT (Fig. 2E), suggesting there was no postoperative tendon rupture or slackening.

718

719 ***Data recordings***

720 EMG signals were recorded using the AlphaLab SnR system (Alpha Omega
721 Engineering, Hamerkava St. 6, Ziporit Industrial Zone, P.O.Box 810, Nof HaGalil

(Nazareth Illit) 1789062, Israel), displayed online and then stored on a hard drive for later off-line analysis using MATLAB (MathWorks, Natick, MA, USA). Data were recorded at 11 kHz and processed for analysis as follows. 1. Down-sampled to 5 kHz; 2. 50 Hz high-pass filtered (6th order Butterworth filter); 3. rectified; 4. 20 Hz low-pass filtered (6th order Butterworth filter); and 5. down-sampled to 100 Hz. Behavioral task events were recorded as transistor–transistor logic (TTL) signals using the AlphaLab SnR system. Monkey behavior was further recorded by two cameras (Sanyo VPC-WH1, 60 fps [Sanyo, Osaka, Japan]; and Casio EX-100F, 240 fps [Casio, Tokyo, Japan] for monkeys A and B, respectively) from two different angles (top and side view). The images were later used to detect additional behavioral events (contact time with the object and pull onset for Monkey A; and food touch and food lift onset for Monkey B), and detection of possible changes in the animal's general movement pattern. Kinovea software was used for this video analysis (free and open-source software; https://www.kinovea.org/).

740 ***Behavioral task***

741 Before and after EMG surgery, the monkeys were trained on a simple grasping
742 task that involved a small object attached to a rod (Fig. 3B for Monkey A; and Fig.
743 4B for Monkey B). For Monkey A, object 1 was a small rod placed between two
744 side walls encouraging the monkey to grasp the rod with a precision grip using
745 the tips of the index finger and thumb (controlled grasp). The force used to
746 compress the spring while pulling was low and the distance moved short. Object
747 2 had to be grasped in the same way. However, the force to compress the spring
748 was higher and the distance moved longer (object 1: 300 cN, 4 mm; and object
749 2: 800 cN, 30 mm). The monkey was asked to grasp and hold the objects for
750 approximately 300–500 ms (Fig. 3A–D). After completing the trial, the monkey
751 was rewarded with a piece of fruit that had to be taken from the experimenter's
752 palm. The task sequence for Monkey A ranged from object 1 hold onset to object
753 2 hold offset (Fig. 3C, D; and 'Data Analysis' below). For Monkey B, object 1 was
754 a small rod that was grasped and pulled (300 cN, 4 mm) using a lateral
755 prehension grip (like using a door key), and resembling a power grip rather than
756 a natural grasp. However, instead of grasping object 2, Monkey B picked up a
757 piece of fruit from an allocated location. In doing so, the monkey had to cross the

path of a photo cell which was detected by the recording system (Fig. 4A–D). The task sequence to be analyzed for Monkey B ranged from object 1 hold onset to food touch, which was indicated by a LED (Fig. 4C, D; and ‘Data Analysis’ below).

For Monkey A, the task sequence was as follows (Fig. 3A; and Supplementary Video S1). From a starting position in front of the monkey, it had to lift its arm and move towards object 1, grasp, pull, and then hold the object for 500 ms. Immediately after releasing object 1, Monkey A proceeded to move its hand towards object 2, which was located to the right of object 1. Again, the monkey had to grasp, pull, and then hold the object for another 500 ms. Each hold period was accompanied by an audio signal which stopped once the hold duration was sufficient. After completing the task, which was signaled by another acoustic signal, the monkey was rewarded with a piece of fruit presented by the experimenter and taken by the monkey.

For Monkey B, the first part of the sequence was identical. However, after releasing object 1, Monkey B was required to pick up a piece of fruit from an allocated location (Fig. 4A, B; and Supplementary Video S5). In doing so, the monkey passed a photocell in front of the food well. This event was detected by

775 the recording system and a video camera (a red LED triggered by activation of
776 the photocell). For the analysis, only object 1 and the food grasp were considered
777 in monkeys A and B, respectively.

778

779 ***Data analysis***

780 *EMG analysis*

781 EMG data were normalized to the average time for each monkey to complete a
782 trial (object 1 hold onset ➔ object 2 hold offset/LED offset = 100%). Data were
783 cropped and aligned according to the time stamps (Obj1 hold offset ± 15%; and
784 LED onset [food touch] ± 15% for monkeys A and B, respectively). Recorded
785 EMGs from the pre- and post-tendon surgery period were averaged for each
786 recording and compared over experimental sessions. For both monkeys, the
787 muscles used for EMG analysis were: FDS and EDC for pre- (control) and EDC
788 for post-TT (experimental).

789 Both monkeys required time to recover from surgery. Once they were able to
790 perform the task on their own, data collection started (29 and 20 days post-

791 surgery for monkeys A and B, respectively). After tendon surgery, EMG signals
792 for FDS, FCU, and FCR deteriorated in Monkey B. Therefore, there is no
793 experimental data for these muscles in this monkey and they were excluded from
794 the muscle synergy analysis.

795

796 *Synergy analysis*

797 The EMG envelopes obtained from pre-processing raw EMG data were divided
798 by the mean value to normalize activity. Muscle synergies were then extracted
799 for each session using NMF (d'Avella et al., 2003). NMF decomposes the EMG
800 data matrix M, as a product of two matrices C and W:

801 $$M = CW^T + re = \Sigma c_i {w_i}^T + re$$

802 where the vector wi and column of matrix W are muscle synergies; the vector ci,
803 and column of matrix C are their temporal coefficients; and re represents the
804 residuals. Multiplicative update rules were used for decomposition (Lee and
805 Seung, 1999). Updating matrices for decomposition from 20 different random
806 initial matrices was started, and factorization results with least residuals among

807 the 20 results were used. To improve robustness of the muscle synergies, one
808 set of muscle synergies was extracted from EMG data of multiple trials of each
809 day. A k-fold cross validation was used, with k = 4 i.e., EMG data set of multiple
810 trials during the day was split into four data sets, in which three data sets were
811 for training and one data set was for testing. Synergy matrix W was calculated
812 from three training data sets using NMF, and then a coefficient matrix C was
813 calculated by decomposing the EMG matrix M of the test data set with a fixed W
814 matrix of the training data set. This operation was repeated by changing the test
815 data set for each four data sets. Finally, the extracted four C matrices and four W
816 matrices were averaged to obtain daily synergies.

817 The number of synergies was determined as the number where VAF exceeded
818 a threshold. This threshold was set as 0.8. To clarify the effect of TT, the number
819 of synergies for each monkey was determined, assuming that trial-by-trial
820 variation in synergies within the same monkey was small. MATLAB 'nnmf'
821 function was used for NMF.

822

823 To determine whether the weights of muscle synergies changed after TT, the
824 following procedure was used. First, the average of each pre-TT spatial synergy

825 was calculated and used as control data to calculate the cosine distance for all
826 post-TT spatial synergies. This generated four distance relationships for each
827 pre-TT synergy. If the change in spatial synergy before and after TT was small,
828 then only one of the four cosine distances (e.g., synergy A before TT and synergy
829 A after TT) should be significantly smaller. Two-way ANOVA was conducted
830 using the type of synergy and session as factors for the cosine distance. The
831 significance of synergy pairs was identified using the Bonferroni post-hoc test.
832

833 *Cross-correlation analysis*

834 Cross-correlation analysis was performed to examine pre- and post-surgery EMG
835 signals as well as temporal activation coefficients of extracted muscle synergies.
836 Cross-correlation coefficients were calculated using MATLAB (MathWorks,
837 corrcoef.m function). These were plotted for different muscles and muscle
838 synergy activation coefficients over experimental sessions for comparison.

839 Based on cross-correlation analysis, five 'landmark days' were identified for
840 further analysis (Fig. 6P). These days represent distinct stages in the recovery
841 process and excluded pre-surgery control data. The first landmark day was

842 chosen from one of the initial recording sessions after TT surgery (days 29 and
843 22 in monkeys A and B, respectively) when the cross-correlation coefficients had
844 changed significantly compared with control data. The second day was then
845 chosen from a time period just before the switch-back, when the cross-correlation
846 coefficients had started to return to their original values (days 64 and 36). Another
847 day was then picked from the period when the coefficients were still changing
848 significantly (days 69 and 44) and before starting to saturate. At this point the next
849 day was defined (days 79 and 48). Finally, the final landmark day was chosen
850 from one of the last recording sessions when the behavior had fully recovered
851 (days 99 and day 64 for monkeys A and B, respectively).

852

853 *Behavioral analysis*

854 To examine behavioral recovery, the duration, onset, and offset of object and
855 food grasps were analyzed. Event times extracted from the video analysis were
856 used for alignment of EMG data and subsequent cross-correlation and synergy
857 analyses, along with recorded event TTL signals. For each experimental session,
858 the first 20 trials of each video recording were analyzed. In Monkey A, the
859 following events were detected and in-between times stored in ms: touch onset,

860 pull onset, and hold onset (resulting in grasp duration and pull time) for object 1
861 and object 2. In Monkey B, the following events were detected and in-between
862 times stored: touch onset, pull onset, and hold onset (resulting in grasp duration
863 and pull time) for object 1; and for the food grasp component of the task, LED
864 onset, food-touch onset, food-lift onset, LED offset, and movement end (contact
865 of food with mouth).

866 Contact times (touch onset ➔ pull onset) for Monkey A were plotted in ms (mean
867 ± SD) over number of days from tendon surgery for object 1. For Monkey B,
868 contact times with food (food-touch ➔ food-lift onset) were plotted in ms (mean
869 ± SD).

870 ANOVA was performed to compare control data recorded before and after tendon
871 surgery. In total, 5 and 3 control sessions vs. 35 and 22 experimental sessions
872 were used for analyses in monkeys A and B, respectively.

873 To quantify the observed aberrant reaching behavior, video footage was
874 analyzed and the means of 10 consecutive trials calculated for each session as
875 follows. For Monkey A, time spent within a specific spatial window covering the
876 area behind and between the two objects was measured; the monkey passed

through this space almost exclusively while exhibiting the impairment (see Fig. 3E, crossing of the yellow dotted line). In Monkey B, the time spent in contact with the rear plate of the object was measured (see Fig. 4G).

Joint kinematics analysis

To determine whether compensatory movements occurred, steady state changes in joint angles were examined before and after recovery. Using DeepLabCut (Mathis et al., 2018; Nath et al., 2019), key points on the fingers and wrists were tracked from experimental videos. From the obtained key points, the vector v_1 connecting the wrist and fingers and vector v_2 connecting the arm and wrist were estimated. The joint angle θ was calculated as follows:

$$cos(\Theta) = \frac{\underline{v_2} \cdot \underline{v_3}}{|\underline{v_2}|\,|\underline{v_3}|} \rightarrow \Theta = cos^{-1}\left(\frac{\underline{v_2} \cdot \underline{v_3}}{|\underline{v_2}|\,|\underline{v_3}|}\right)$$

DATA, MATERIALS, AND SOFTWARE AVAILABILITY

Matlab scripts and raw data will be made available online. All study data are included in the article and/or SI Appendix.

ACKNOWLEDGEMENTS:

We would like to express our sincere gratitude to Drs. Francisco Valero-Cuevas and Andrea d'Avella for their invaluable comments and constructive suggestions on the earlier version of the manuscript, and Drs Nicholas Schweighofer and Gerald E. Loeb for stimulating discussion. We would also like to thank Dr. Naomichi Ogihara and Prof. Toshiyasu Nakamura for their valuable insights and technical advice on tendon surgery in the hand and forearm of primates. We are grateful to Drs. Kumiko Oida and Chika Sasaki for their medical care of the experimental animals, vital help during surgery, and training of the animals. Lastly, we would like to thank Masahi Koizumi for designing parts of the experimental setup and Drs. Joachim Confais, Shinji Kubota, Saeka Tomatsu, Tatsuya Umeda, and Natsumi Uchida for their support and assistance during the proceeding pilot study. We thank Rachel James, PhD, from Edanz (https://jp.edanz.com/ac) for editing a draft of this manuscript.

This work was supported by Grants-in-Aid for Scientific Research from the Ministry of Education, Culture, Sports, Science, and Technology of Japan (26120003, 26250013, 15K21754, 19H05724, 19H01092, 23H05488, and 24K21313), the Japan Agency for Medical Research and Development

(JP24gm0010009), the Japan Science Technology Agency Precursory Research for Embryonic Science and Technology program, commissioned research (no. 22102) from the National Institute of Information and Communications Technology, and commissioned research by National Institute of Information and Communications Technology (NICT), Japan (all to K.S.). This work is also supported in part by the NSF CRCNS Japan-US 2113096 to K.S. (Subaward PI) and Francisco Valero-Cueva (PI). The content is solely the responsibility of the authors and does not necessarily represent the official views of the NSF.

REFERENCES

Berger DJ, Gentner R, Edmunds T, Pai DK, d'Avella A (2013) Differences in Adaptation Rates after Virtual Surgeries Provide Direct Evidence for Modularity. The Journal of Neuroscience 33:12384-12394.

Berniker M, O'Brien MK, Kording KP, Ahmed AA (2013) An Examination of the Generalizability of Motor Costs. PLOS ONE 8:e53759.

Bizzi E, Cheung VC (2013) The neural origin of muscle synergies. Frontiers in Computational Neuroscience Volume 7 - 2013.

Bowlus TH, Lane RD, Stojic AS, Johnston M, Pluto CP, Chan M, Chiaia NL, Rhoades RW (2003) Comparison of reorganization of the somatosensory system in rats that sustained forelimb removal as neonates and as adults. J Comp Neurol 465:335-348.

Cash DJW, Jones JWM (2011) The role of tenodesis in surgery of the upper limb. The Journal of Bone & Joint Surgery British Volume 93-B:285-292.

Cheung VC, Turolla A, Agostini M, Silvoni S, Bennis C, Kasi P, Paganoni S, Bonato P, Bizzi E (2012) Muscle synergy patterns as physiological markers of motor cortical damage. Proc Natl Acad Sci U S A 109:14652-14656.

d'Avella A, Saltiel P, Bizzi E (2003) Combinations of muscle synergies in the construction of a natural motor behavior. Nature Neuroscience 6:300-308.

Davidson PR, Wolpert DM (2003) Motor learning and prediction in a variable environment. Curr Opin Neurobiol 13:232-237.

De Nunzio AM, Schweisfurth MA, Ge N, Falla D, Hahne J, Gödecke K, Petzke F, Siebertz M, Dechent P, Weiss T, Flor H, Graimann B, Aszmann OC, Farina D (2018) Relieving phantom limb pain with multimodal sensory-motor training. J Neural Eng 15:066022.

Dieterich AV, Botter A, Vieira TM, Peolsson A, Petzke F, Davey P, Falla D (2017) Spatial variation and inconsistency between estimates of onset of muscle activation from EMG and ultrasound. Sci Rep 7:42011.

Edwards MJ, Adams RA, Brown H, Pareés I, Friston KJ (2012) A Bayesian account of 'hysteria'. Brain 135:3495-3512.

Flash T, Sejnowski TJ (2001) Computational approaches to motor control. Curr Opin Neurobiol 11:655-662.

Fleury L, Prablanc C, Priot AE (2019) Do prism and other adaptation paradigms really measure the same processes? Cortex 119:480-496.

Foell J, Bekrater-Bodmann R, Diers M, Flor H (2014) Mirror therapy for phantom limb pain: brain changes and the role of body representation. Eur J Pain 18:729-739.

Gaetz W, Dockstader C, Furlong PL, Amaral S, Vossough A, Schwartz ES, Roberts TPL, Scott Levin L (2023) Somatosensory and motor representations following bilateral transplants of the hands: A 6-year longitudinal case report on the first pediatric bilateral hand transplant patient. Brain Res 1804:148262.

Gardenier J, Garg R, Mudgal C (2020) Upper Extremity Tendon Transfers: A Brief Review of History, Common Applications, and Technical Tips. Indian J Plast Surg 53:177-190.

Gijsberts A, Bohra R, Sierra González D, Werner A, Nowak M, Caputo B, Roa MA, Castellini C (2014) Stable myoelectric control of a hand prosthesis using non-linear incremental learning. Front Neurorobot 8:8.

Green HJ (1997) Mechanisms of muscle fatigue in intense exercise. J Sports Sci 15:247-256.

Hatem SM, Saussez G, Della Faille M, Prist V, Zhang X, Dispa D, Bleyenheuft Y (2016) Rehabilitation of Motor Function after Stroke: A Multiple

Systematic Review Focused on Techniques to Stimulate Upper Extremity Recovery. Front Hum Neurosci 10:442.

Hoffmann G, Kamper DG, Kahn JH, Rymer WZ, Schmit BD (2009) Modulation of stretch reflexes of the finger flexors by sensory feedback from the proximal upper limb poststroke. J Neurophysiol 102:1420-1429.

Hospod V, Aimonetti J-M, Roll J-P, Ribot-Ciscar E (2007) Changes in Human Muscle Spindle Sensitivity during a Proprioceptive Attention Task. The Journal of Neuroscience 27:5172-5178.

Hunter DJ, Eckstein F (2009) Exercise and osteoarthritis. J Anat 214:197-207.

Jami L (1992) Golgi tendon organs in mammalian skeletal muscle: functional properties and central actions. Physiol Rev 72:623-666.

Kakavas G, Brilakis E, Papatzikou M, Malliaropoulos N, Mazeas J, Forelli F (2025) Reverse Linear Neuro Periodization Model for Rehabilitation After Arthroscopic Rotator Cuff Repair: A Narrative Review. Clinics and Practice 15:105.

Kitago T, Krakauer JW (2013) Motor learning principles for neurorehabilitation. Handb Clin Neurol 110:93-103.

Kitago T, Ryan SL, Mazzoni P, Krakauer JW, Haith AM (2013) Unlearning

versus savings in visuomotor adaptation: comparing effects of washout, passage of time, and removal of errors on motor memory. Front Hum Neurosci 7:307.

Kitazawa S, Kohno T, Uka T (1995) Effects of delayed visual information on the rate and amount of prism adaptation in the human. J Neurosci 15:7644-7652.

Lee DD, Seung HS (1999) Learning the parts of objects by non-negative matrix factorization. Nature 401:788-791.

Levin MF, Weiss PL, Keshner EA (2015) Emergence of virtual reality as a tool for upper limb rehabilitation: incorporation of motor control and motor learning principles. Phys Ther 95:415-425.

Loeb GE (1999) Asymmetry of hindlimb muscle activity and cutaneous reflexes after tendon transfers in kittens. J Neurophysiol 82:3392-3405.

Luauté J, Schwartz S, Rossetti Y, Spiridon M, Rode G, Boisson D, Vuilleumier P (2009) Dynamic changes in brain activity during prism adaptation. J Neurosci 29:169-178.

Maier M, Ballester BR, Verschure PFMJ (2019) Principles of Neurorehabilitation After Stroke Based on Motor Learning and Brain Plasticity Mechanisms.

Frontiers in Systems Neuroscience Volume 13 - 2019.

Martin TA, Keating JG, Goodkin HP, Bastian AJ, Thach WT (1996) Throwing while looking through prisms. II. Specificity and storage of multiple gaze-throw calibrations. Brain 119 (Pt 4):1199-1211.

Mathis A, Mamidanna P, Cury KM, Abe T, Murthy VN, Mathis MW, Bethge M (2018) DeepLabCut: markerless pose estimation of user-defined body parts with deep learning. Nature Neuroscience 21:1281-1289.

Mercuri E, Muntoni F (2013) Muscular dystrophies. Lancet 381:845-860.

Morton SM, Bastian AJ (2006) Cerebellar contributions to locomotor adaptations during splitbelt treadmill walking. J Neurosci 26:9107-9116.

Murata Y, Higo N, Oishi T, Yamashita A, Matsuda K, Hayashi M, Yamane S (2008) Effects of motor training on the recovery of manual dexterity after primary motor cortex lesion in macaque monkeys. J Neurophysiol 99:773-786.

Mussa-Ivaldi FA, Bizzi E (1995) The Modular Organization of Motor Control: What Frogs Can Teach Us About Adaptive Learning. IFAC Proceedings Volumes 28:413-418.

Nath T, Mathis A, Chen AC, Patel A, Bethge M, Mathis MW (2019) Using

DeepLabCut for 3D markerless pose estimation across species and behaviors. Nature Protocols 14:2152-2176.

Nordez A, Gallot T, Catheline S, Guével A, Cornu C, Hug F (2009) Electromechanical delay revisited using very high frame rate ultrasound. J Appl Physiol (1985) 106:1970-1975.

Nudo RJ, Wise BM, SiFuentes F, Milliken GW (1996) Neural substrates for the effects of rehabilitative training on motor recovery after ischemic infarct. Science 272:1791-1794.

Overduin SA, d'Avella A, Roh J, Bizzi E (2008) Modulation of Muscle Synergy Recruitment in Primate Grasping. The Journal of Neuroscience 28:880-892.

Petitet P, O'Reilly JX, O'Shea J (2018) Towards a neuro-computational account of prism adaptation. Neuropsychologia 115:188-203.

Popa LS, Streng ML, Hewitt AL, Ebner TJ (2016) The Errors of Our Ways: Understanding Error Representations in Cerebellar-Dependent Motor Learning. Cerebellum 15:93-103.

Power JD, Schlaggar BL (2017) Neural plasticity across the lifespan. Wiley Interdiscip Rev Dev Biol 6.

Ranganathan R, Adewuyi A, Mussa-Ivaldi FA (2013) Learning to be lazy: exploiting redundancy in a novel task to minimize movement-related effort. J Neurosci 33:2754-2760.

Sattin D, Parma C, Lunetta C, Zulueta A, Lanzone J, Giani L, Vassallo M, Picozzi M, Parati EA (2023) An Overview of the Body Schema and Body Image: Theoretical Models, Methodological Settings and Pitfalls for Rehabilitation of Persons with Neurological Disorders. Brain Sci 13.

Schärli A, Hecht H, Mast FW, Hossner EJ (2024) How spotting technique affects dizziness and postural stability after full-body rotations in dancers. Hum Mov Sci 95:103211.

Schoultz TW, Swett JE (1972) The fine structure of the Golgi tendon organ. J Neurocytol 1:1-26.

Slawinska U, Kasicki S (2002) Altered Electromyographic Activity Pattern of Rat Soleus Muscle Transposed into the Bed of Antagonist Muscle. The Journal of Neuroscience 22:5808-5812.

Smith MA, Shadmehr R (2005) Intact ability to learn internal models of arm dynamics in Huntington's disease but not cerebellar degeneration. J Neurophysiol 93:2809-2821.

1069 Smith MA, Ghazizadeh A, Shadmehr R (2006a) Interacting Adaptive Processes
1070 with Different Timescales Underlie Short-Term Motor Learning. PLOS
1071 Biology 4:e179.
1072 Smith MA, Ghazizadeh A, Shadmehr R (2006b) Interacting adaptive processes
1073 with different timescales underlie short-term motor learning. PLoS Biol
1074 4:e179.
1075 Smith SA, Mitchell JH, Garry MG (2006c) The mammalian exercise pressor
1076 reflex in health and disease. Exp Physiol 91:89-102.
1077 Sperry RW (1940) The functional results of muscle transposition in the hind limb
1078 of the rat. Journal of Comparative Neurology 73:379-404.
1079 Sperry RW (1942) Transplantation of motor nerves and muscles in the forelimb
1080 of the rat. Journal of Comparative Neurology 76.
1081 Sugita Y (1996) Global plasticity in adult visual cortex following reversal of
1082 visual input. Nature 380:523-526.
1083 Takei T, Seki K (2010) Spinal interneurons facilitate coactivation of hand
1084 muscles during a precision grip task in monkeys. J Neurosci 30:17041-
1085 17050.
1086 Takei T, Confais J, Tomatsu S, Oya T, Seki K (2017) Neural basis for hand

1087 muscle synergies in the primate spinal cord. Proceedings of the National
1088 Academy of Sciences 114:8643-8648.
1089 Takeuchi N, Izumi S (2012) Maladaptive plasticity for motor recovery after
1090 stroke: mechanisms and approaches. Neural Plast 2012:359728.
1091 Tannenbaum J, Bennett BT (2015) Russell and Burch's 3Rs then and now: the
1092 need for clarity in definition and purpose. J Am Assoc Lab Anim Sci
1093 54:120-132.
1094 Thompson AK, Wolpaw JR (2014) Operant conditioning of spinal reflexes: from
1095 basic science to clinical therapy. Front Integr Neurosci 8:25.
1096 Trewartha KM, Garcia A, Wolpert DM, Flanagan JR (2014) Fast but fleeting:
1097 adaptive motor learning processes associated with aging and cognitive
1098 decline. J Neurosci 34:13411-13421.
1099 Vallbo AB, Hagbarth KE, Torebjörk HE, Wallin BG (1979) Somatosensory,
1100 proprioceptive, and sympathetic activity in human peripheral nerves.
1101 Physiol Rev 59:919-957.
1102 van Vliet P, Carey LM, Turton A, Kwakkel G, Palazzi K, Oldmeadow C, Searles
1103 A, Lavis H, Middleton S, Galloway M, Dimech-Betancourt B, O'Keefe S,
1104 Tavener M (2023) Task-specific training versus usual care to improve

upper limb function after stroke: the “Task-AT Home” randomised controlled trial protocol. Frontiers in Neurology 14.

Vanhoof MJM, van Leeuwen T, Galletta L, Vereecke EE (2021) The forearm and hand musculature of semi-terrestrial rhesus macaques (Macaca mulatta) and arboreal gibbons (fam.Hylobatidae). Part II. Quantitative analysis. Journal of Anatomy 238:321-337.

Villalta JI, Landi SM, Fló A, Della-Maggiore V (2013) Extinction Interferes with the Retrieval of Visuomotor Memories Through a Mechanism Involving the Sensorimotor Cortex. Cerebral Cortex 25:1535-1543.

Walker JG, Jackson HJ, Littlejohn GO (2004) Models of adjustment to chronic illness: using the example of rheumatoid arthritis. Clin Psychol Rev 24:461-488.

Wester K, Hove LM, Barndon R, Craven AR, Hugdahl K (2018) Cortical Plasticity After Surgical Tendon Transfer in Tetraplegics. Front Hum Neurosci 12:234.

Winterbottom L, Nilsen DM (2024) Motor Learning Following Stroke: Mechanisms of Learning and Techniques to Augment Neuroplasticity. Phys Med Rehabil Clin N Am 35:277-291.

Wolpert DM (1997) Computational approaches to motor control. Trends Cogn Sci 1:209-216.

Yan Y, Sobinov AR, Bensmaia SJ (2022) Prehension kinematics in humans and macaques. J Neurophysiol 127:1669-1678.

Yumiya H, Larsen KD, Asanuma H (1979) Motor readjustment and input-output relationship of motor cortex following cross-connection of forearm muscles in cats. Brain Research 177:566-570.

Zajac FE (1992) How musculotendon architecture and joint geometry affect the capacity of muscles to move and exert force on objects: a review with application to arm and forearm tendon transfer design. J Hand Surg Am 17:799-804.

Zeiler SR, Krakauer JW (2013) The interaction between training and plasticity in the poststroke brain. Curr Opin Neurol 26:609-616.

Zemková E (2022) Physiological Mechanisms of Exercise and Its Effects on Postural Sway: Does Sport Make a Difference? Front Physiol 13:792875.

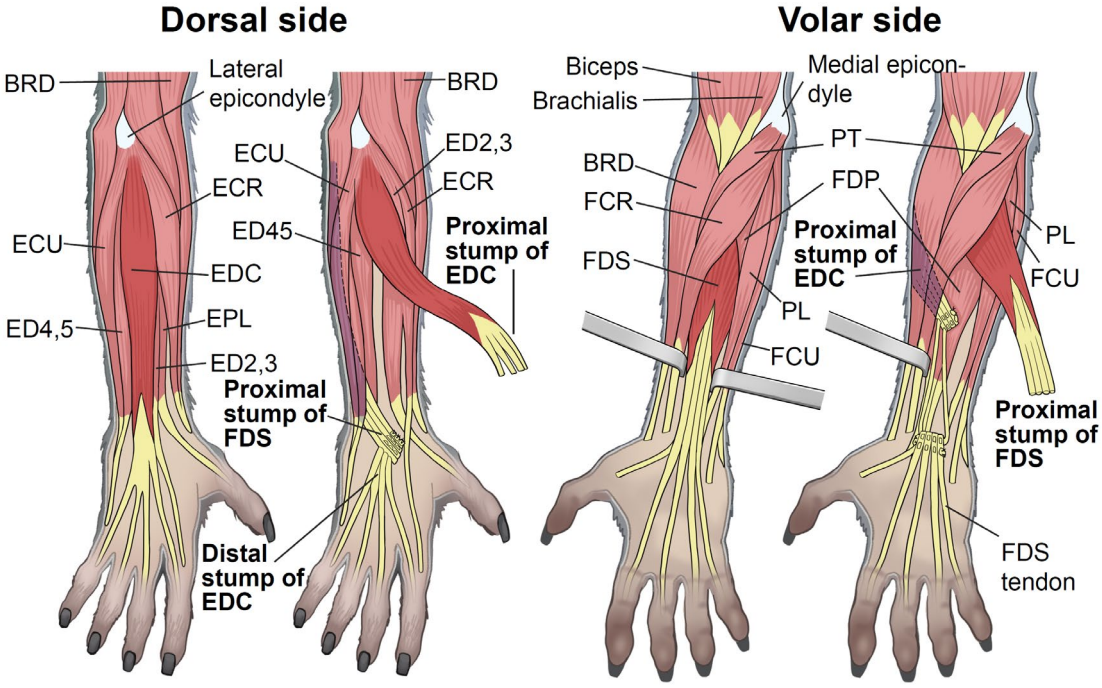

Figure 1: Muscle anatomy of the macaque forearm and the tendon transfer procedure.

A schematic of the primary forearm muscles involved in the study, showing both the dorsal and volar views. The diagram illustrates the surgical crossed tendon transfer of the extensor digitorum communis (EDC) and flexor digitorum superficialis (FDS) tendons. All labeled muscles were implanted with EMG electrodes. Muscle Abbreviations: BRD: brachioradialis, ECR: extensor carpi radialis, ECU: extensor carpi ulnaris, ED2,3: extensor digitorum-2,3, ED4,5: extensor digitorum-4,5, EPL: extensor pollicis longus, FCR: flexor carpi radialis, FCU: flexor carpi ulnaris, FDP: flexor digitorum profundus, PL: palmaris longus, PT: pronator teres, *(The deltoid (DEL) muscle was also implanted in Monkey B but is not shown as it is a shoulder muscle.)*

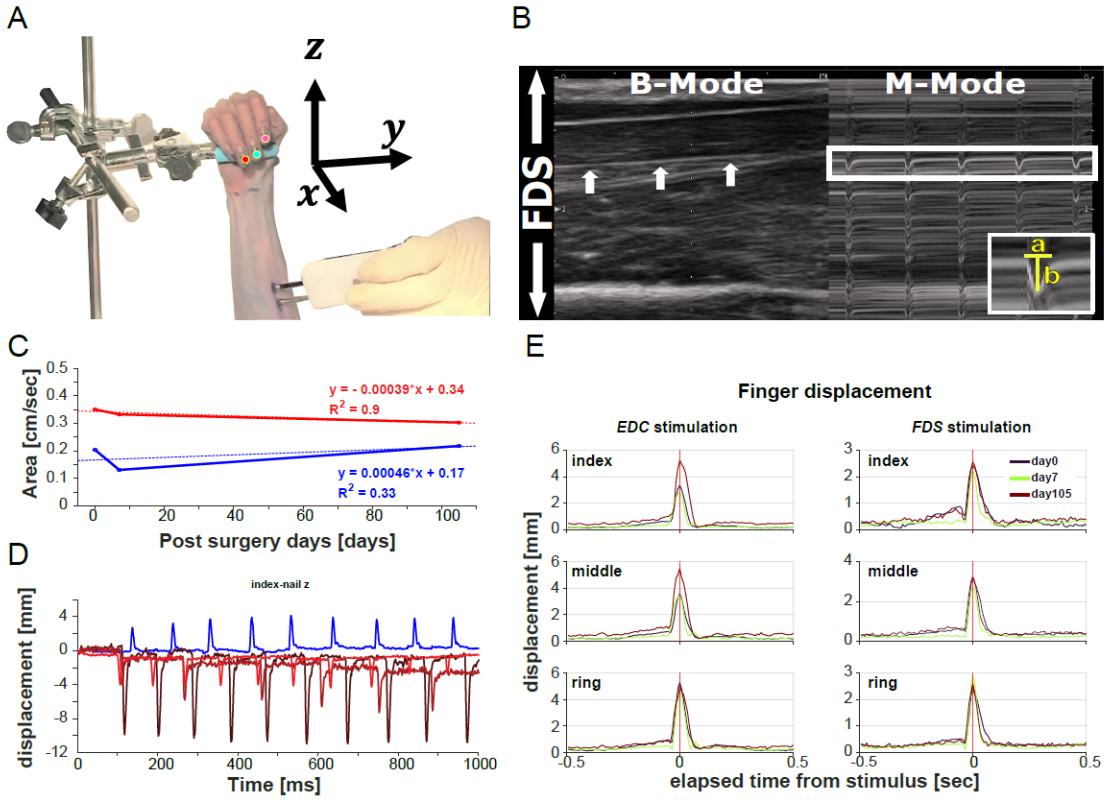

Figure 2: ***Long term confirmation of tendon surgery effectiveness to alter mechanical properties.***

(A) Set-up for the ultrasound measurement and video recordings of the stimulation induced movements of the EDC and FDS tendons. (B) Sonogram of the FDS muscle and its intramuscular tendons. Left side (B-mode, i.e., brightness mode) shows the still image of the monkeys forearm at a given point in time. Right side (M-mode, i.e., motion mode) shows the stagged images of the FDS tendon displacement induced by muscle stimulation (50mA). White arrows demarcate the FDS tendon which was used for the measurement. Grayscale gradations correspond to tissue densities: hyperechoic regions (white) denote denser structures like surface of bones and tendons, while hypoechoic areas (black) signify less dense tissues such as adipose tissue and musculature. Inset demonstrates the area measurement. The area of the displacement waves was measured in the M-mode, representing the strength of muscle contraction. We measured the duration (a, sec) and amplitude (b, cm) of three waves and calculated the average. Area = a*b/2(cm/sec) for days 0, 7 and 105 after tendon transfer. (C) Areas under the wave measured in the M-mode for 3 experimental days (0, 7 and 105 days post-TT) and regression lines in red and blue for FDS

and EDC, respectively. R2>0.5 for FDS. The data suggested that muscle contractions induced by direct electrical stimulation were nearly constant. (D) Markers placed on the index, middle and ring finger nails (A) were used to measure finger displacement in xyz-dimensions. We calculated the sum of the Euclidean distances of each marker from the origin of the 3D coordinate system as a scalar quantity. Observing the movement along the Z-axis, it became reversed post-surgery indicating a reversal from finger flexion to extension due to tendon transfer (D, blue = pre-TT at surgery day; dark brown = post-TT at surgery day; light brown = 1wk post-TT; red = 3wks post-TT). The scalar quantity of the fingers during muscle stimulation did not change much at day 0, 7 and 105 days (E), suggesting that there was no tendon rupture or slackening of the tendons postoperatively (EDC stimulation, left; FDS stimulation, right).

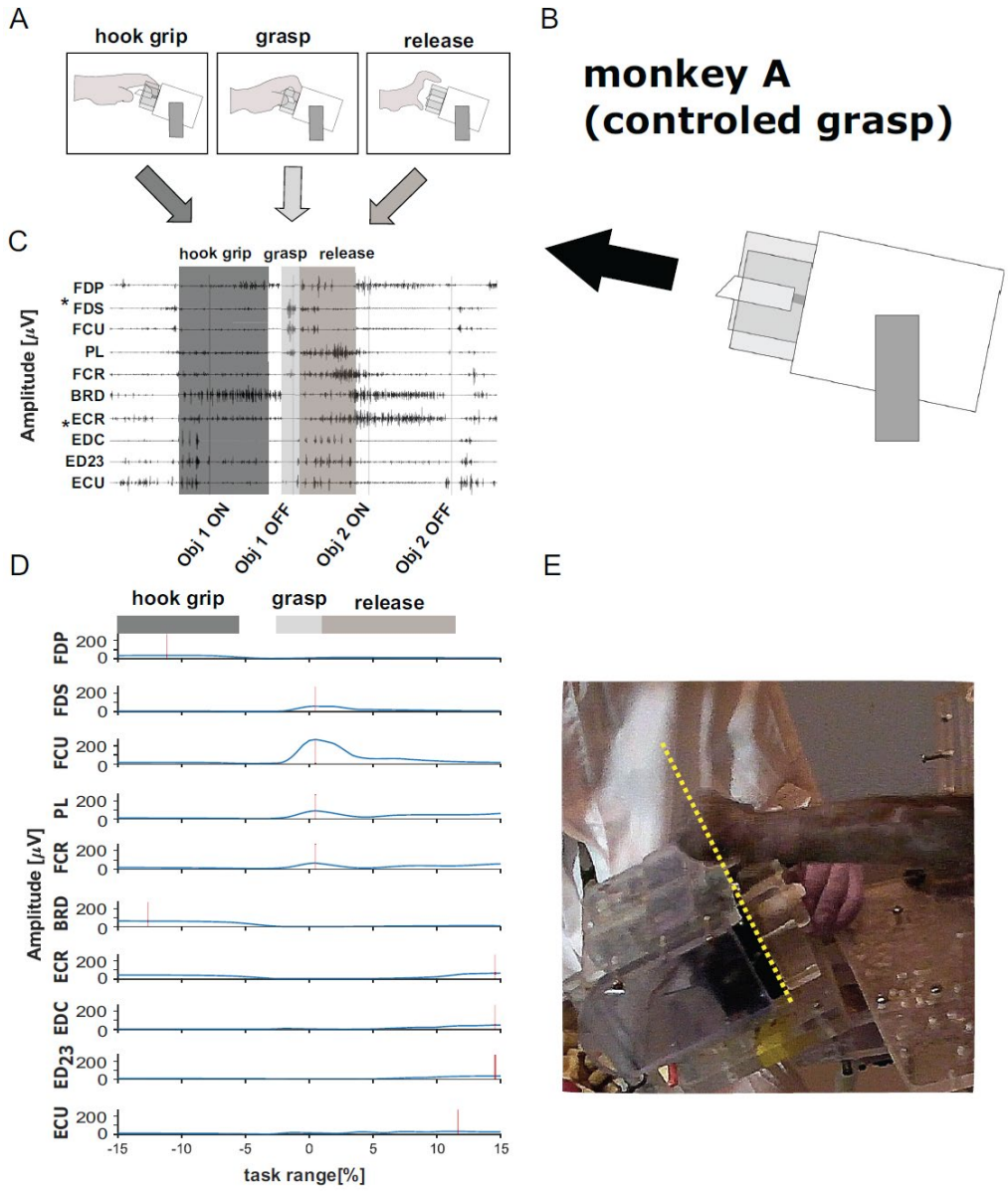

Figure 3: ***Experimental set-up, task sequence and typical EMG (monkey A).***

(A) Schematic of the behavioral sequence (hook → grasp → release). (B) Schematic of the task object using a rod requiring monkey A to perform a controlled grasp. (C) Typical EMG traces of a control session (high-pass filtered) for all recorded muscles. Gray boxes represent the task sequence. Obj 1 ON: start of the hold period of object 1. Obj 1 OFF: end of the hold period of object 1, i.e., object release. Obj 2 ON: start of the hold period of object 2. Obj 2 OFF: end of the hold period of object 2, i.e., object release. Tendons of the muscles marked with * were cross-transferred. (D) Rectified and smoothed EMG for all recorded

muscles (average for one recording session; amplitude [μV] over task sequence [%]). Horizontal bars illustrate the corresponding behavioral periods, red vertical lines indicate peak amplitude for each muscle). (E) The time the monkey spent on the left side of the yellow dotted line while moving from object 1 to object 2 was measured and used to quantify the mal-adaptive behavior.

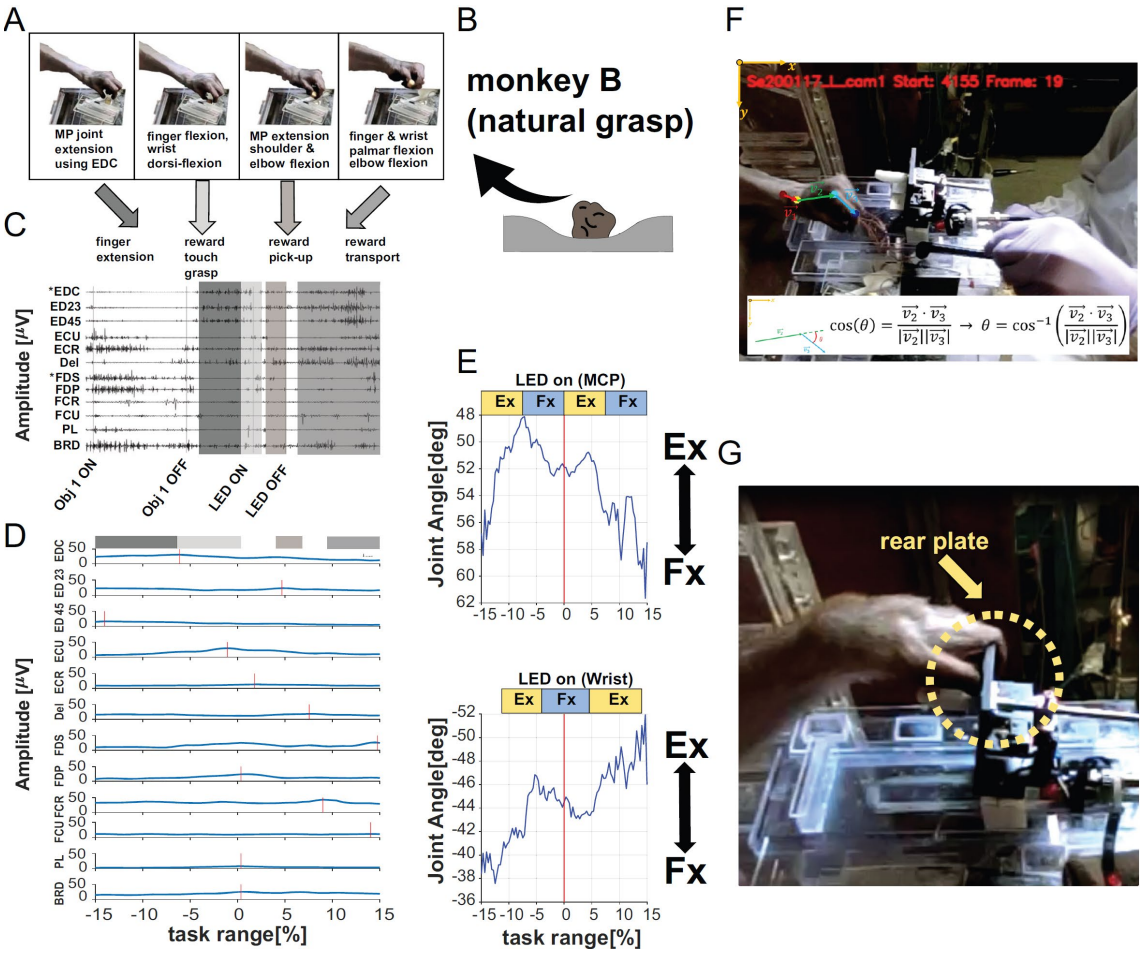

Figure 4: Experimental set-up, task sequence and typical EMG (monkey B).

(A) Schematic of the task sequence (picking up food). (B) Schematic of the task requiring monkey B to pick up food from a groove allowing for a more natural grasp. (C) Typical EMG traces of a control session (high-pass filtered) for all recorded muscles. Gray boxes represent the task. Obj 1 ON: start of the hold period of object 1. Obj 1 OFF: end of object 1's hold period, i.e. object release. LED ON: approximate start of the food touch. LED OFF: approximate time of food retrieval. Tendons of the muscles marked with * were cross-transferred. (D) rectified and smoothed EMG for all recorded muscles (average for one recording session; amplitude [μV] over task sequence [%]). Horizontal bars illustrate the corresponding behavioral periods, red vertical lines indicate peak amplitude for each muscle). (E) Development of the metacarpophalangeal joint (MCP) and wrist joint angle [deg] over task range [%]. Decreasing and increasing angles indicate extension or flexion of the MCP or wrist angle, respectively. Data are aligned on LED onset (food retrieval) and indicate consistency between

behavioral observation (A), EMG (C-D) and kinematics (E). (F) Illustration of joint angle measurement using a still picture of the monkey while performing the task. (G) Example for mal-adaptive behavior in monkey B. The time the monkey spent in contact with or behind the object plate was measured and used to quantify the mal-adaptive behavior.

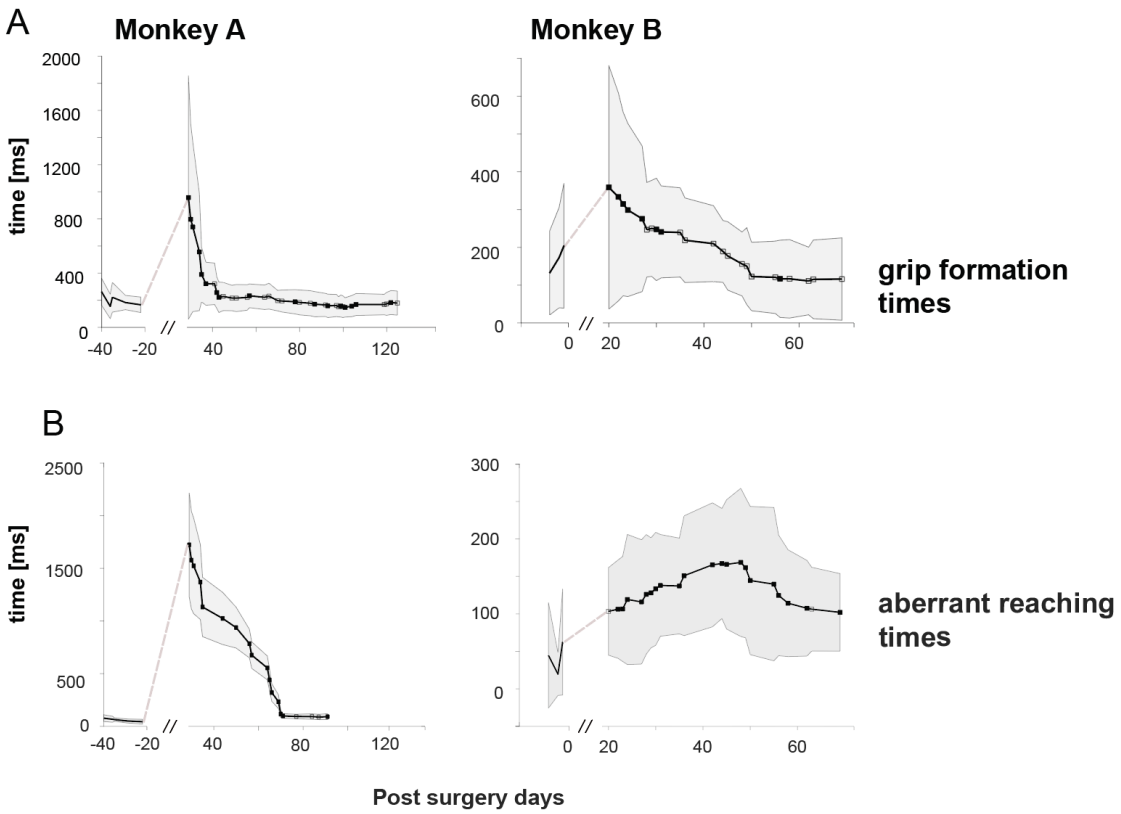

Figure 5: ***Behavioral recovery is preceded by maladaptive motor control in both monkeys.***

(A) Grip formation times. Plotted is the average time (mean ± SD, n=20 trials) from initial touch to action onset (pull or lift) for Monkey A and Monkey B. Grip formation times were significantly elevated immediately post-surgery before returning to baseline. (B) Quantification of aberrant reaching. Plotted is the average time (mean ± SD, n=10 trials) spent executing aberrant movements. For Monkey A, this was the duration spent moving behind the target (see Fig. 3E); for Monkey B, it was the duration in contact with the object's rear plate (see Fig. 4G). These behaviors were prominent in the early post-surgical phase and diminished over time. Filled squares indicate a significant difference from pre-TT baseline ($p<0.05$, two-sample t-test). All data are plotted over days relative to the tendon transfer (TT) surgery (day 0).

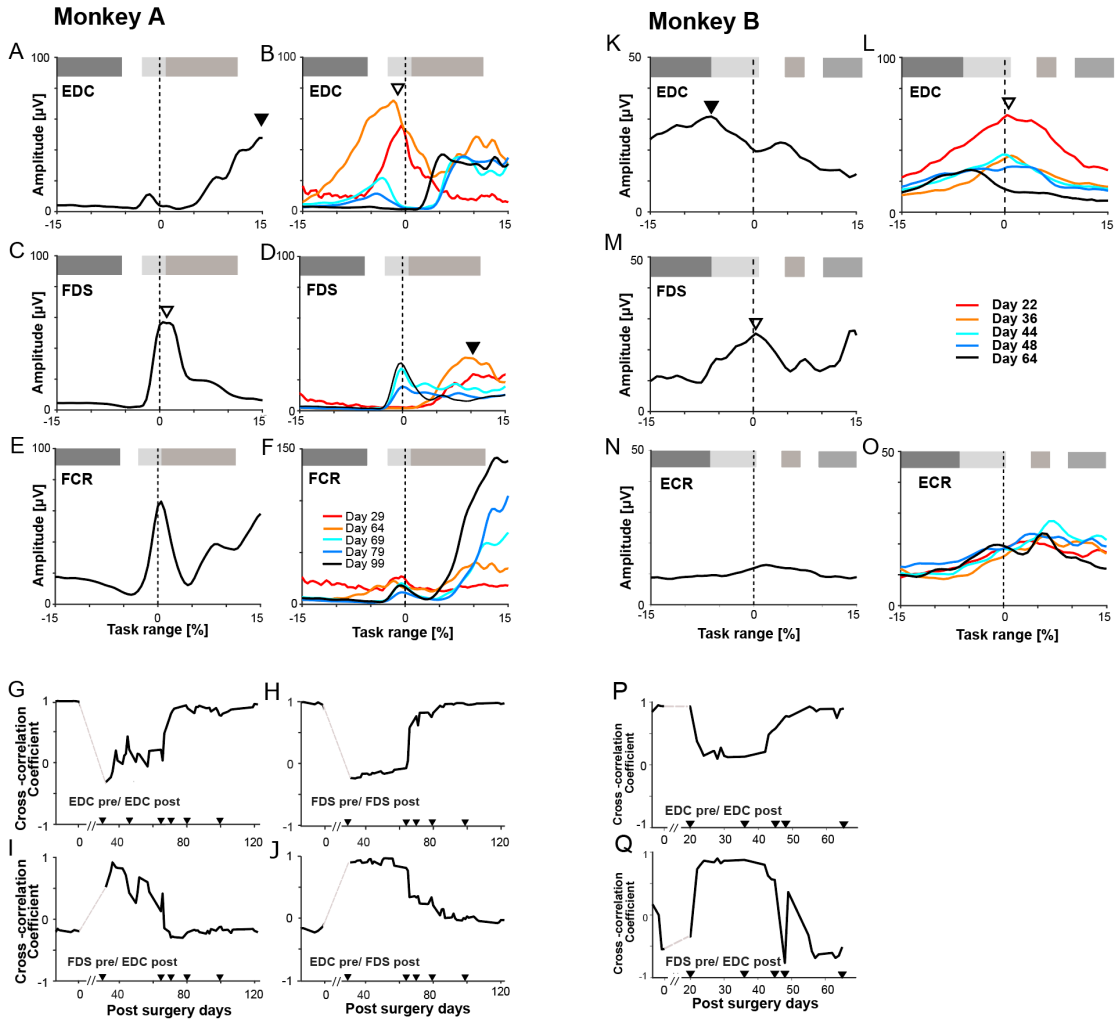

Figure 6: A *Two-Phase Adaptation of Muscle Activity is Observed in Both Monkeys Following Tendon Transfer.*

The figure compares EMG activity profiles and cross-correlation analyses for Monkey A (left) and Monkey B (right), demonstrating a consistent pattern of motor adaptation consisting of an initial functional swap followed by a later reversion. A representative non-transferred muscle is included for each monkey. Monkey A (A-J): Profiles are aligned on object release. Monkey B (K-Q): Profiles are aligned on food touch. Filled triangles (▼) indicate peak activity occurring during finger extension, while open triangles (▽) indicate peak activity occurring during finger flexion. Small triangles on correlation plots denote landmark days.

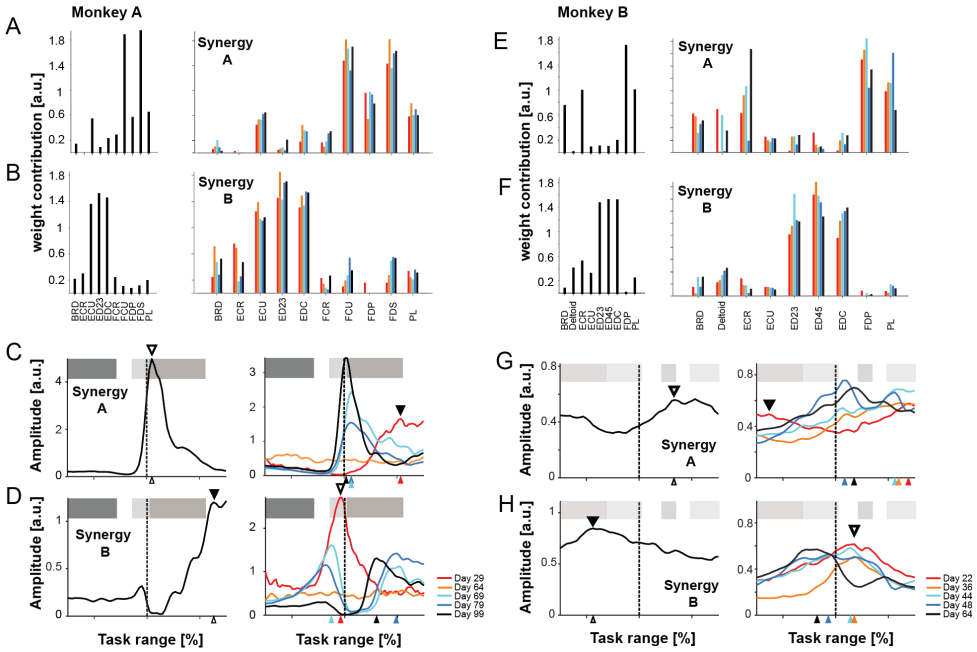

Figure 7: Muscle Synergy Compositions Remain Stable While Their Activation Timings Show a Two-Phase Adaptation.

The figure presents the spatial muscle weights and temporal activation coefficients for the primary finger flexor (Synergy A) and extensor (Synergy B) for Monkey A (A-D) and Monkey B (E-H). (A, B, E, F) Spatial Synergy Weights: The muscle weight contributions for each synergy are shown for the pre-surgery control period and for five post-surgery landmark days, demonstrating that synergy structure was preserved. (C, D, G, H) Temporal Activation Coefficients: The activation profiles show the same two-phase adaptation seen in individual muscles: an initial swap followed by a later reversion. Symbols and alignment are as described in Fig. 6.

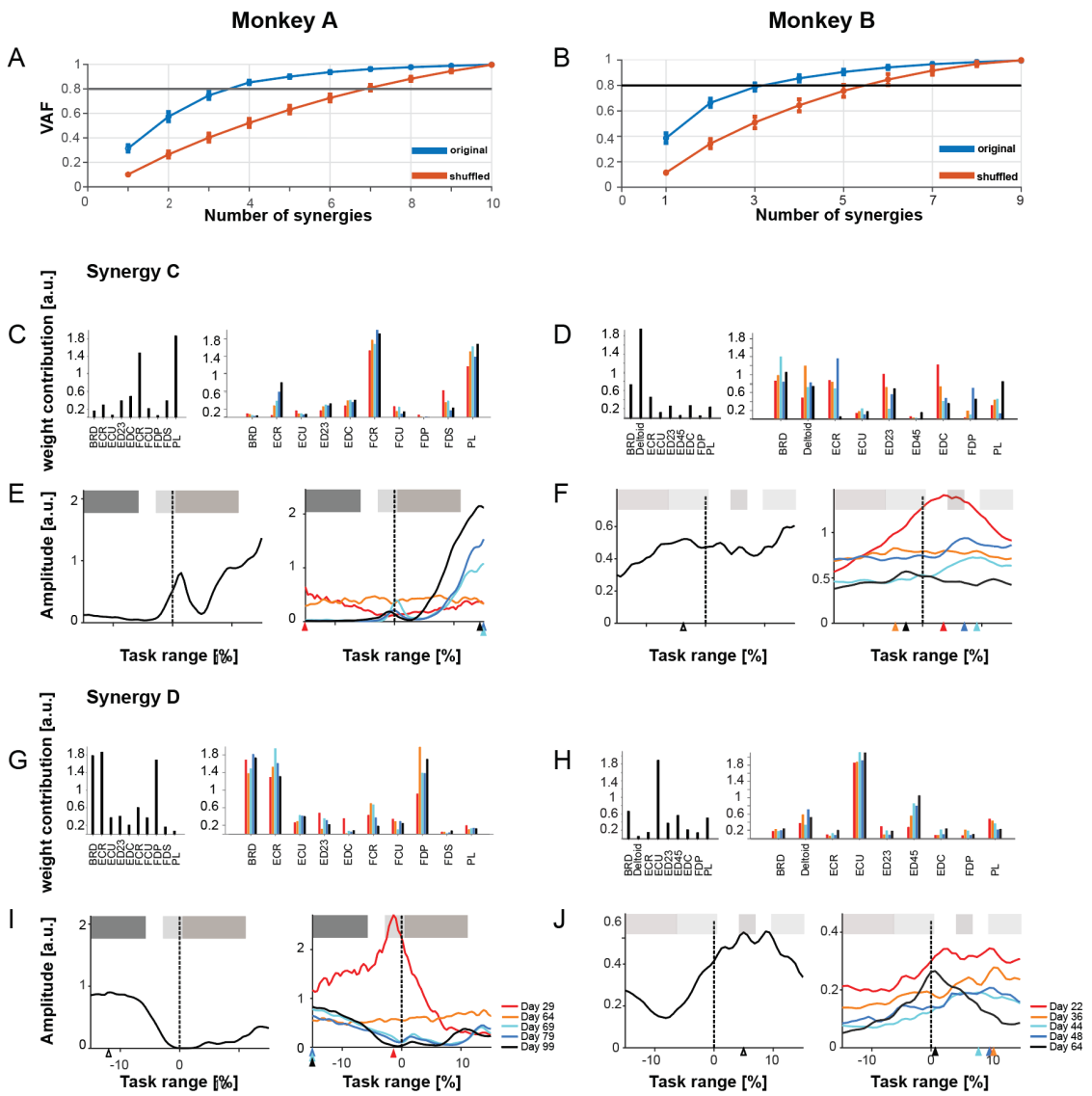

Figure 8: Analysis of Secondary Muscle Synergies and Variance Accounted For (VAF).

This figure provides supporting data for the synergy analysis, including the VAF plots justifying the use of four synergies, and the detailed analysis of the secondary Synergies C and D for both Monkey A and Monkey B. (A-B) Variance Accounted For (VAF). The plots show the cumulative variance in the EMG data explained by an increasing number of synergies for Monkey A (left) and Monkey B (right). In both original datasets (blue lines), four synergies were sufficient to account for more than 80% of the variance (demarcated by the black horizontal line), justifying the dimensionality of the synergy model. VAF for corresponding

shuffled data is shown for comparison (red lines). (C-F) Analysis of Synergy C (Wrist Flexor Synergy). This panel group shows the spatial weights (C, D) and temporal activation coefficients (E, F) for Synergy C in Monkey A and Monkey B, respectively. Spatial Weights (C, D): Pre-surgery control profiles (left sub-panels) are compared to post-surgery landmark days (right sub-panels), demonstrating that the muscle contributions to this synergy remained largely stable. Temporal Activation (E, F): In Monkey A, the temporal profile (C) shows a notable increase in activation during the late adaptation phase, consistent with its recruitment for a compensatory strategy. The adaptive pattern for Monkey B (E) was less distinct. (G-J) Analysis of Synergy D. This panel group shows the spatial weights (G, H) and temporal activation coefficients (I, J) for Synergy D in Monkey A and Monkey B. This synergy, which contributes to wrist extension, exhibited relatively minor and inconsistent changes following the tendon transfer in both animals. For all temporal plots, profiles are aligned on object release (Monkey A) or food touch (Monkey B) at 0% task range. Post-surgery plots show data from selected landmark days as indicated by the color legend.

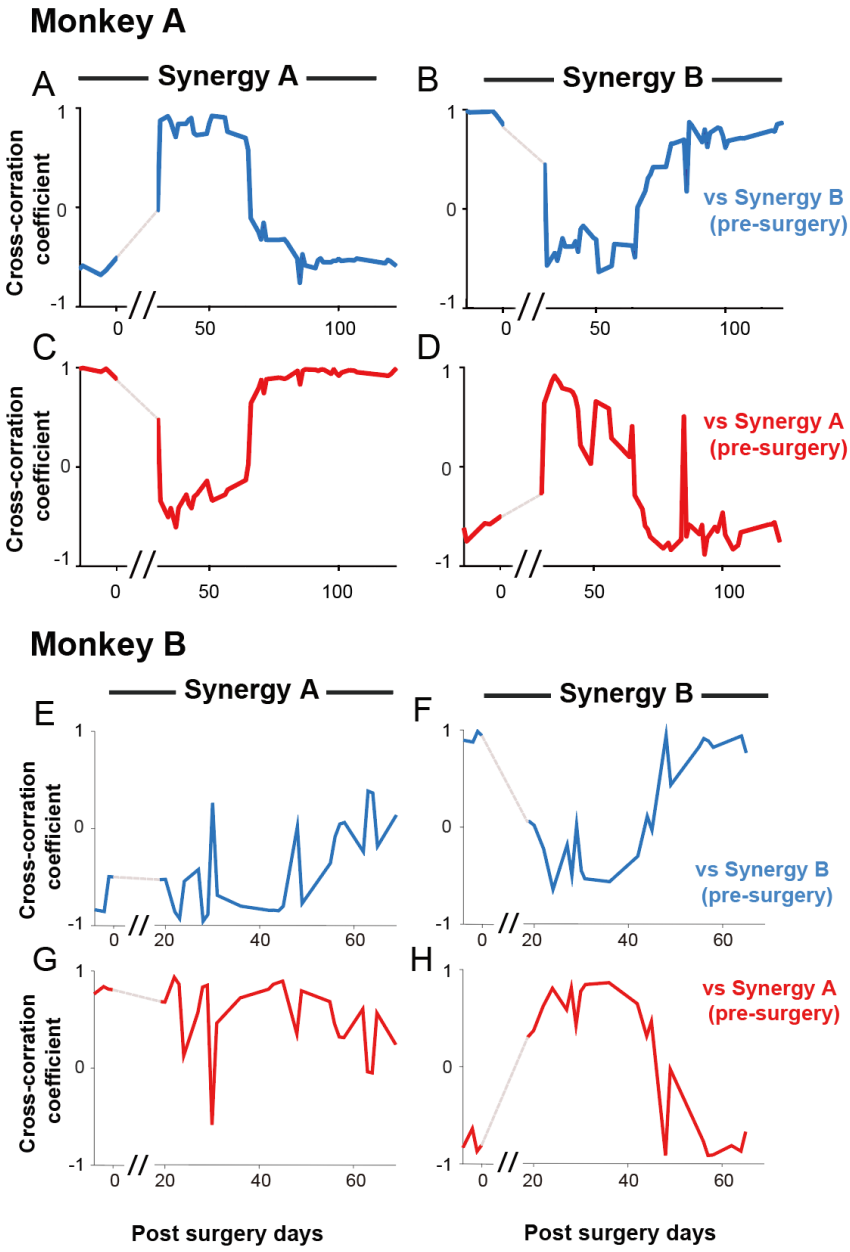

Figure 9: Cross-correlation analysis reveals the two-phase adaptation of primary synergy activation.-

Cross-correlation coefficients for the primary flexor (Synergy A) and extensor (Synergy B) synergies are plotted over post-surgery days for Monkey A (A-D) and Monkey B (E-H). For each synergy, the activation pattern was cross-correlated with its own pre-surgery profile (A, B, E, F) and with that of its antagonist (C, D, G, H). The results quantitatively demonstrate the swap-and-revert pattern in both animals. The // represents the recovery period.

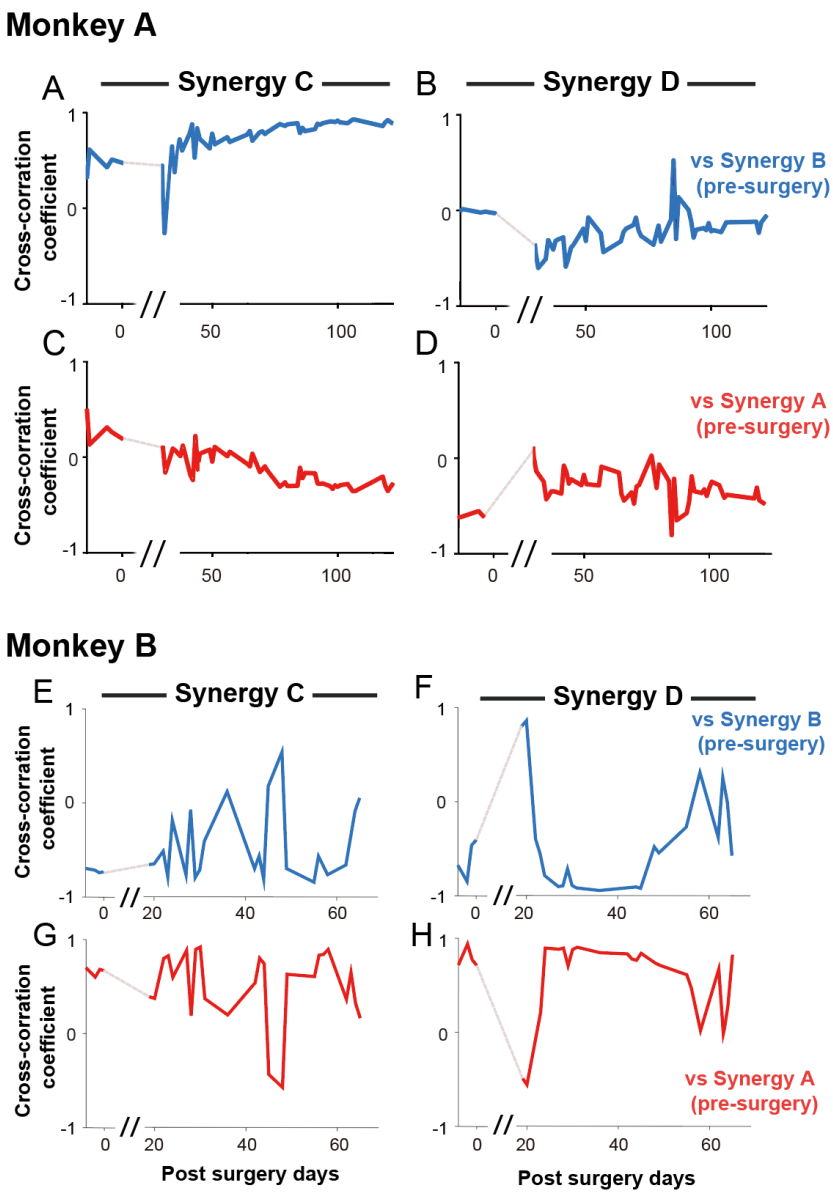

Figure 10: Cross-correlation analysis of secondary synergy activation.

Cross-correlation coefficients for the secondary synergies (C and D) are plotted over post-surgery days for Monkey A (A-D) and Monkey B (E-H). For each synergy, the activation pattern was cross-correlated with the pre-surgery profiles of Synergy A (red lines) and Synergy B (blue lines) to reveal their changing relationships to the primary flexor and extensor commands.

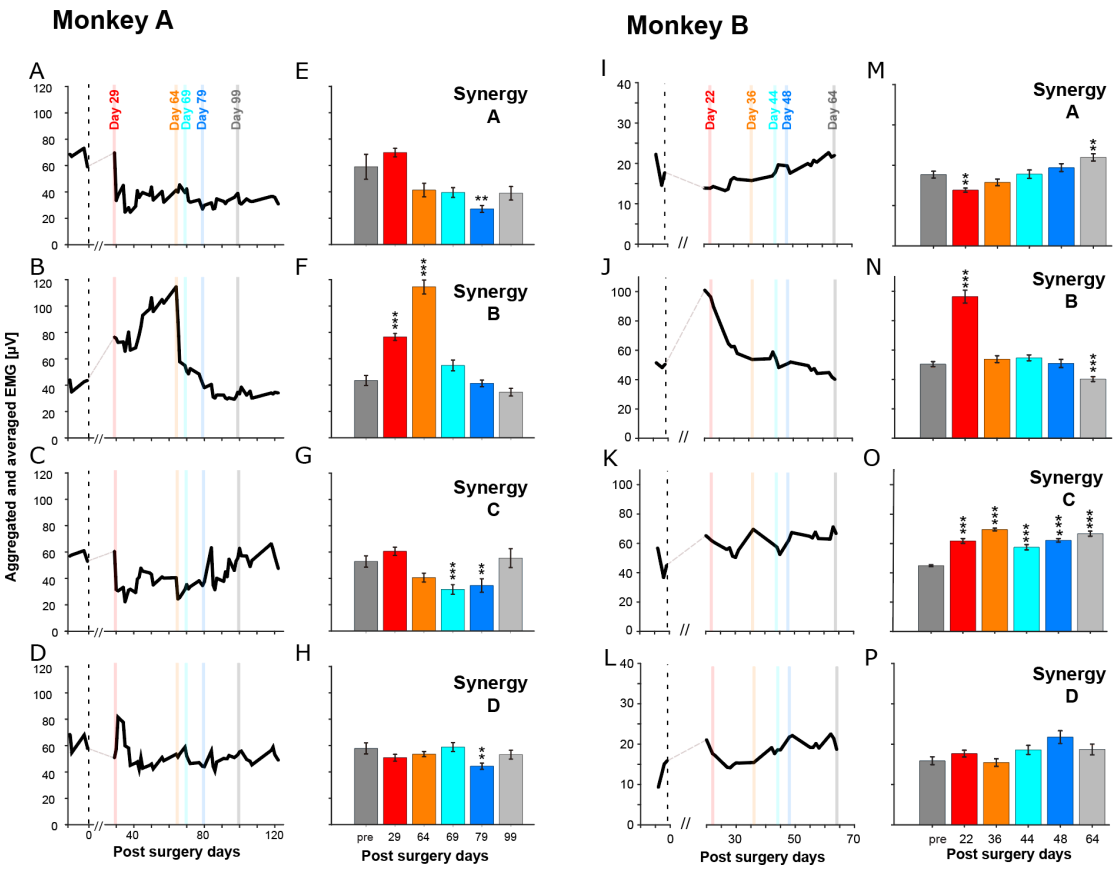

Figure 11: Aggregated and averaged EMG (aaEMG) reveals synergy-specific adaptive patterns.

Aggregated and averaged electromyography (EMG) activities for the main contributing muscles of each of the four synergies for Monkey A (A-H) and Monkey B (I-P). For each recording session, EMG activity within a ±15% task range window was summed for the contributing muscles and then averaged. The left columns for each monkey (A-D, I-L) show the aaEMG over all post-surgery days. The right columns (E-H, M-P) show the mean (± SEM) aaEMG for the pre-surgery period ("pre") and the five selected landmark days. Monkey A (A-H) The contributing muscles for each synergy were: Synergy A: flexor digitorum superficialis (FDS) and flexor carpi ulnaris (FCU). Synergy B: extensor digitorum communis (EDC), extensor digitorum-2,3 (ED23), and extensor carpi ulnaris (ECU). Synergy C: palmaris longus (PL) and flexor carpi radialis (FCR). Synergy D: flexor digitorum profundus (FDP), brachioradialis (BRD), and extensor carpi radialis (ECR). Monkey B (I-P) The contributing muscles for each synergy were: Synergy A: flexor digitorum profundus (FDP) and palmaris longus (PL). Synergy B: extensor digitorum communis (EDC), extensor digitorum-2,3 (ED23) and

extensor digitorum-4,5 (ED45). Synergy C: extensor carpi radialis (ECR), brachioradialis (BRD), and deltoid (DEL). Synergy D: extensor carpi ulnaris (ECU). Vertical colored bars on the time-series plots indicate the landmark days shown in the bar plots. The // on the time axis represents the recovery period during which no recordings were taken. Asterisks on bar plots indicate a significant difference from the pre-surgery control period ($p < 0.01$, $^{*}p < 0.001$, $^{**}p < 0.0001$; two-sample t-test with Bonferroni correction, $\alpha = 0.01$).

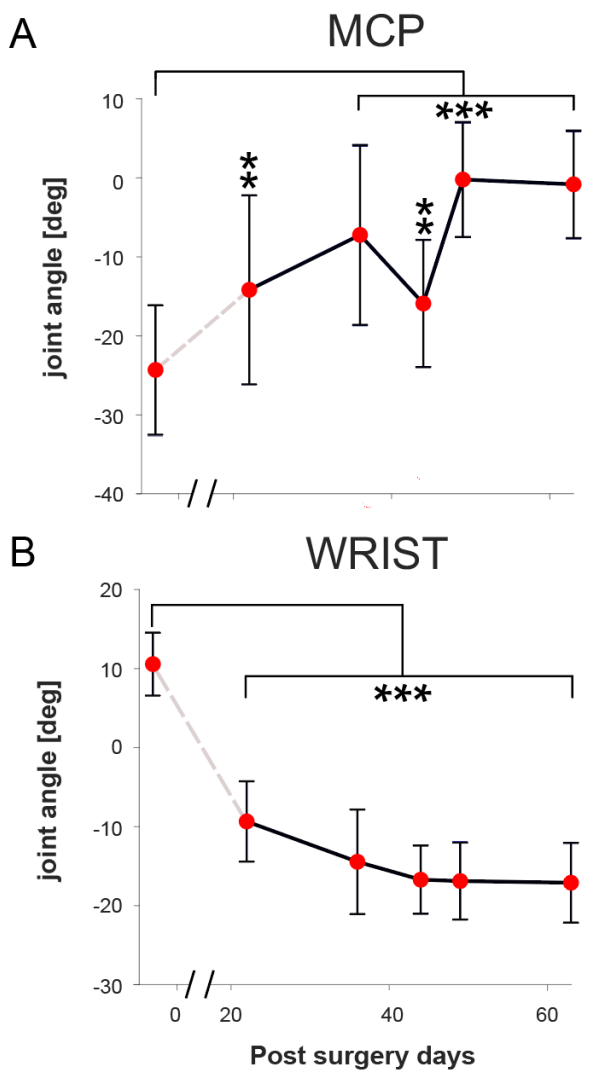

Figure 12: Kinematic analysis reveals a compensatory tenodesis strategy in Monkey B.

Changes in joint angles at the wrist and metacarpophalangeal (MCP) joint for Monkey B (mean of 20 trials ±SD for each landmark day, taken 83ms before food touch). (A) The MCP joint angle increased post-surgery, indicating greater finger extension. (B) Concurrently, the wrist joint angle decreased, indicating wrist flexion. This coordinated movement pattern is characteristic of an active tenodesis effect, suggesting it was used as a compensatory strategy to achieve finger extension. Statistical analysis confirmed these changes were significant ($p < 0.0001$, $\alpha = 0.01$, ANOVA).

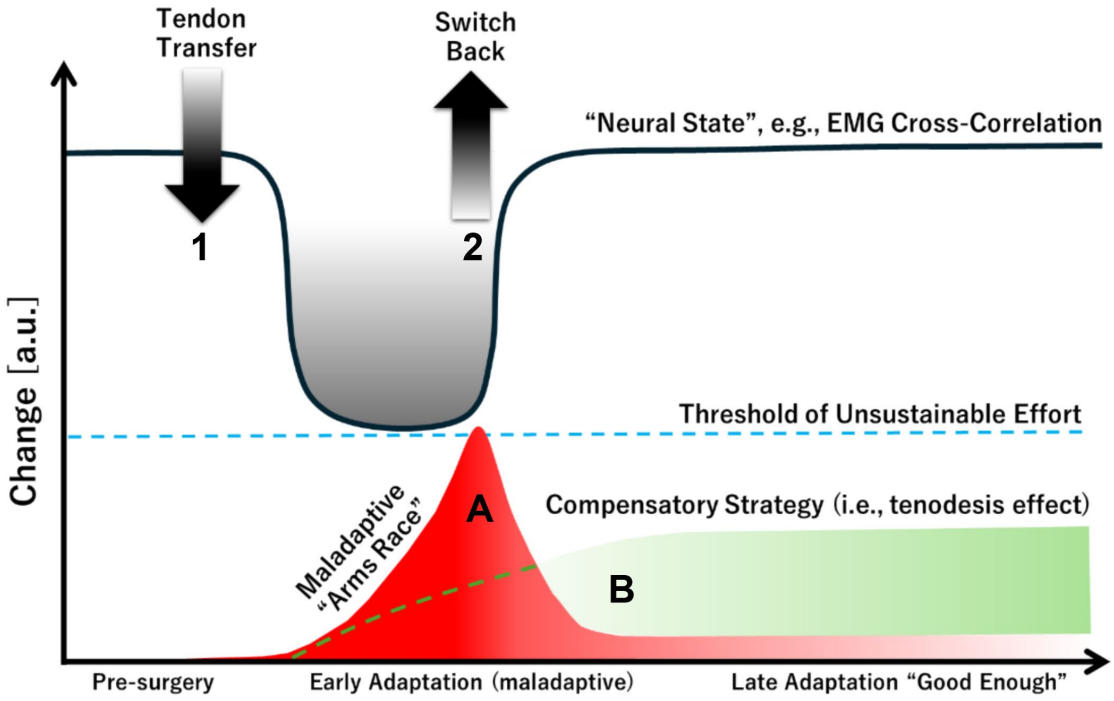

Figure 13: A Proposed Model of Multi-Timescale Adaptation Following Tendon Transfer.

This schematic illustrates the hypothesized interaction between fast and slow adaptive processes driving recovery. The initial Tendon Transfer triggers a rapid but maladaptive 'swap' of motor commands (Fast Adaptation 1), leading to a maladaptive state. During this phase, two slower processes are hypothesized to occur in parallel: a costly 'arms race' within the conflicted synergy (Slow Process A, red curve) and the gradual development of a functional compensatory strategy (Slow Process B, green curve). When the 'arms race' reaches a threshold of unsustainable cost (dashed blue line), a second Fast Adaptation ('Switch-Back', 2) is triggered. This allows for the abandonment of the flawed strategy and the adoption of a stable, 'good enough' solution, which is now supported by the newly learned compensatory strategy. The gray line represents the observed neural data (e.g., cross-correlation coefficients of electromyography and temporal activation coefficients of muscle synergies), which reflects this two-phase process.